Stem Cell Transplantation Rescued A Primary Open-Angle Glaucoma Mouse Model

Siqi Xiong[1,2], Ajay Kumar[1], Shenghe Tian[1], Eman E. Taher[1,3,] Enzhi Yang[1], Paul R. Kinchington[1], Xiaobo Xia[2*], Yiqin Du[1,4,5*]

1. Department of Ophthalmology, University of Pittsburgh, Pittsburgh, PA 15213
2. Department of Ophthalmology, Xiangya Hospital, Central South University, Changsha, Hunan, China 410008
3. Research Institute of Ophthalmology, Giza, Egypt 12557
4. Department of Developmental Biology, University of Pittsburgh, Pittsburgh, PA 15213
5. McGowan Institute for Regenerative Medicine, University of Pittsburgh, Pittsburgh, PA 15213

*Corresponding authors:

Yiqin Du, duy@upmc.edu; 910 Eye and Ear Institute, 203 Lothrop St, Pittsburgh, PA 15213. Tel: 412-802-8437

Xiaobo Xia, xbxia21@163.com, 87 Xiangya Road, Changsha, Hunan, China 410008. Tel: 011-86-731-84327209

Abstract

Glaucoma is a leading cause of irreversible blindness. In this study, we investigated if exogenous stem cells are able to rescue a glaucoma mouse model with transgenic myocilin Y437H mutation and explored the possible mechanisms. Human trabecular meshwork stem cells (TMSCs) were intracamerally transplanted which reduced mouse intraocular pressure, increased outflow facility and preserved the retinal ganglion cell function. TMSC transplantation also significantly increased the TM cellularity, promoted myocilin secretion from TM cells into the aqueous humor, repaired the TM tissue with extracellular matrix modulation and ultrastructural restoration. Co-culturing TMSCs with myocilin mutation TM cells promoted TMSCs differentiating into phagocytic functional TM cells. RNA sequencing on TMSCs and fibroblasts revealed that TMSCs had upregulated genes related to TM regeneration while fibroblasts had upregulated genes associated to glaucoma. Our results uncovered therapeutic potential of TMSCs for curing glaucoma and elucidated possible mechanisms by which TMSCs achieve the treatment effect.

Key Words: Trabecular meshwork, Stem cells, Transplantation, Glaucoma, Intraocular pressure, RNAseq.

Introduction

Primary open-angle glaucoma (POAG), the most common type of glaucoma with a prevalence of 0.5-7.0% in adults, can result in damage of retinal ganglion cells (RGCs) and irreversible vision loss(Broman et al., 2008; Quigley & Broman, 2006) . The progression of POAG has been demonstrated to be correlated with elevated intraocular pressure (IOP)(Heijl et al., 2002), which is associated with reduced trabecular meshwork (TM) cellularity (Alvarado, Murphy, & Juster, 1984; Alvarado, Murphy, Polansky, & Juster, 1981), malfunction of TM phagocytosis(Buller, Johnson, & Tschumper, 1990) and abnormal deposition of extracellular matrix (ECM)(Keller, Aga, Bradley, Kelley, & Acott, 2009). Replacement of the unhealthy TM cells with healthy functioning TM cells derived from stem cells and restoration of TM function offers a novel alternative approach to treat POAG(Abu-Hassan, Li, Ryan, Acott, & Kelley, 2015; Du et al., 2012; Du, Yun, Yang, & Schuman, 2013; Kelley et al., 2009; Zhu et al., 2016).

Trabecular meshwork stem cells (TMSCs) have their special niche located at the anterior TM tissue beneath the Schwalbe's line(Braunger et al., 2014; Raviola, 1982; Yun, Zhou, Wills, & Du, 2016) and have been successfully isolated and characterized (Du et al., 2012; Du et al., 2013; Yun et al., 2018; Yun et al., 2016). TMSCs maintain stem cell characteristics and regenerative capacity after long-term cryopreservation(Kumar, Xu, & Du, 2020) which can be an effective source for cell-based therapy. TMSCs exhibit the preference to home to the TM region in wildtype mice (Du et al., 2013) and to laser-damaged TM tissue after intracameral injection， which is correlated with CXCR4/SDF1 chemokine axis(Yun et al., 2018). Moreover, TMSCs can improve the outflow facility in a mouse model with laser-induced TM damage(Yun et al., 2018). However, the mechanisms for TMSCs repairing the diseased TM and restoring TM function in POAG have not yet been resolved. Intriguingly, the pathogenesis of POAG is apparently different from that of laser induced glaucoma(Liesenborghs et al., 2019). Hence, exploring the therapeutic effect of TMSCs on models of POAG and uncovering mechanisms underlying it are

88 crucial steps for future clinical therapies for treating glaucoma. Liton et. al. (Liton, Luna,
89 Challa, Epstein, & Gonzalez, 2006) described the genome wide expression profile of
90 TM cells, and compared gene expression of human POAG and non-glaucomatous
91 tissue where they described the upregulation of genes related to inflammation and
92 acute-phase response of genes related to antioxidants. They also reported the genes
93 related to TM cell regeneration(Liton et al., 2006). Liu et. al.(Liu et al., 2013) reported
94 the genes upregulated in myocilin (Myoc) associated human POAG TM tissue. We
95 analyzed the RNAseq data from three strains of human TMSCs and fibroblasts to
96 identify the expression differences of genes mentioned above for unveiling the TMSC
97 regeneration mechanisms.
98 Several factors, such as environment and genetics, have been found to contribute
99 to the occurrence and development of POAG(Janssen et al., 2013). Mutations in the
100 gene encoding Myoc have been confirmed to be associated with glaucoma(Tamm,
101 2002), because they can alter the structure of Myoc protein and result in the retention
102 of misfolded Myoc protein in the endoplasmic reticulum (ER) of TM cells. The
103 accumulated protein can then induce ER stress in TM cells, which is related to
104 glaucoma(Peters, Bhattacharya, Clark, & Zode, 2015). ER stress can also lead to TM
105 dysfunction, abnormal synthesis and turnover of ECM and loss of RGCs(Fingert,
106 Stone, Sheffield, & Alward, 2002). A mouse POAG model with transgenic-Myoc
107 Y437H mutation (Tg-MyocY437H) closely mimics the pathophysiology of human
108 Myoc-associated glaucoma(Zhou, Grinchuk, & Tomarev, 2008; Zode et al., 2012;
109 Zode et al., 2011). Here, we report that human TMSCs that are intracamerally
110 transplanted to the Tg-MyocY437H POAG mice, can repopulate the TM cells, repair
111 the abnormal TM tissue and preserve the function of RGCs.
112
113 **Results**
114 **TMSCs Reduce IOP and Increase Outflow Facility of the Tg-MyocY437H Mice**
115 To investigate therapeutic effect of TMSCs on POAG, human TMSCs were injected
116 into the anterior chamber of the Tg-MyocY437H mice when they were at age of 4-

117 month. Age-matched wildtype (WT) mice served as control. The baseline IOP of 4-
118 month old Tg-MyocY437H mice was 16.5± 0.44 mmHg (Figure 1A), which was
119 significantly higher than that of WT mice (12.38±0.41 mmHg, p <0.0001). Tg-
120 MyocY437H mice transplanted with TMSCs started to lower IOP from 1 month after
121 stem cell transplantation, and IOP decreased to 13.30±0.42 mmHg (Tg-TMSC) at 1
122 month. This was close to that seen in WT mice (WT, 12.30±0.45 mmHg, p = 0.4576).
123 The IOP was significantly lower than that in Tg-MyocY437H mice without TMSC
124 transplantation (Tg, 15.23±0.64 mmHg, p = 0.0254) and the IOP of Tg-MyocY437H
125 mice with sham injection (Tg-Sham, 16.00±0.38 mmHg, p = 0.0005). There was no
126 statistically significant difference of IOPs between untreated (Tg, 15.23±0.64 mmHg)
127 and sham injected Tg-MyocY437H mice (Tg-Sham, 16.00±0.38 mmHg, p = 0.6715).
128 Indeed, the IOP of Tg-MyocY437H mice receiving TMSC injection reduced to the
129 same level as WT mice at 2 months after transplantation (Tg-TMSC, 12.65±0.36
130 mmHg vs WT, 13.03±0.39 mmHg, p = 0.9425) and was lower than untreated (Tg,
131 14.96±0.61 mmHg, p = 0.0042) and sham injected Tg-MyocY437H mice (Tg-sham,
132 15.30±0.21 mmHg, p = 0.0006).
133 To further elucidate the way TMSCs reduced IOP in Tg-MyocY437H mice, we
134 examined the outflow facility of the eyes from all groups. As shown in Figure 1B, Tg-
135 MyocY437H mice displayed higher outflow resistance with lower outflow facility (Tg,
136 0.010±0.001 μL/min/mmHg), while the WT mice showed higher outflow facility (WT,
137 0.017±0.001 μL/min/mmHg, p = 0.0219). Tg-MyocY437H mice with TMSC
138 transplantation showed a significant facilitated outflow of aqueous humor (Tg-TMSC,
139 0.016±0.002 μL/min/mmHg) as compared to untreated (Tg, 0.010±0.001
140 μL/min/mmHg, p = 0.0487) and sham injected Tg-MyocY437H mice (Tg-Sham,
141 0.009±0.005 μL/min/mmHg, p = 0.029). This indicated that TMSCs reduced IOP via
142 improvement of the conventional outflow pathway, the TM-Schlemm's canal pathway.
143 Since corneal thickness can affect the accuracy of IOP measurement, anterior
144 OCT was adopted to evaluate the thickness of the cornea, and this revealed that the
145 corneas had the same thickness among all groups (Figure 1C-D). Anterior synechia,

146 which is an important factor for assessing the efficacy and side effect of stem cell
147 transplantation were not found by OCT examination in the mice with intracameral
148 transplantation of TMSCs or sham injection (Figure 1C).

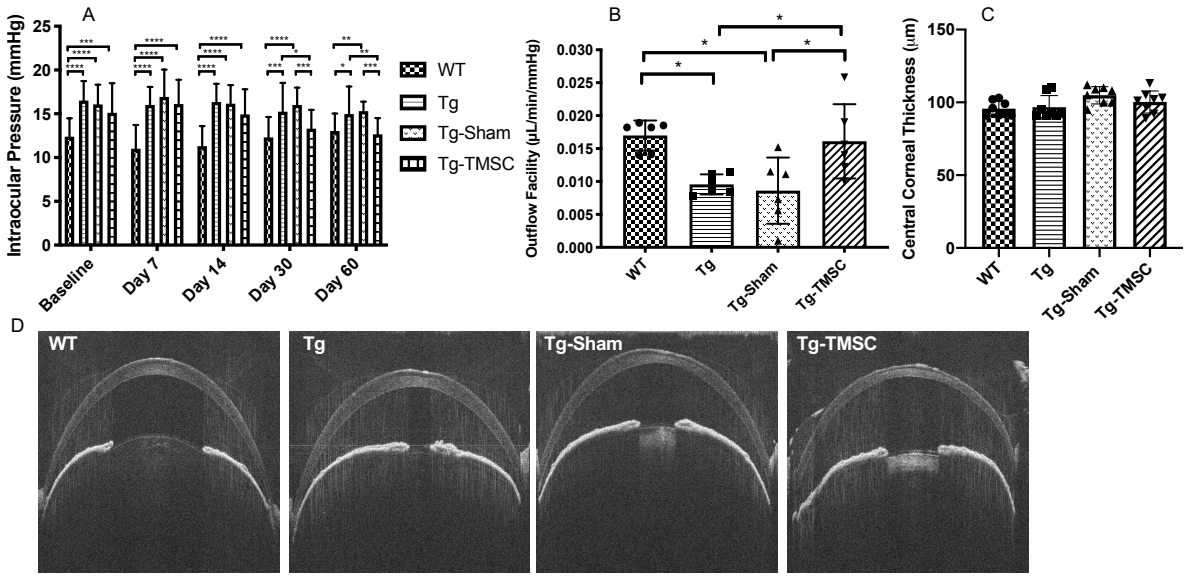

Figure 1. Transplanted TMSCs reduce the intraocular pressure (IOP) and increase outflow facility of Tg-MyocY437H mice. **(A):** IOP was measured before and after intracameral injection at different time points on wildtype mice (WT, n=26), Tg-MyocY437H mice (Tg, n=26), Tg-MyocY437H mice injected with basal medium (Tg-Sham, n=26) and Tg-MyocY437H mice transplanted with TMSC (Tg-TMSC, n=26). **(B):** Outflow facility was evaluated at 2-month after TMSC transplantation to assess the therapeutic effect of TMSCs on repairing the conventional outflow pathway in the Tg-MyocY437H mice comparing to WT, Tg and T-Sham mice（n=6 eyes/group). **(C):** The central corneal thickness was calculated from the images of anterior optical coherence tomography (OCT) to exclude the impact of corneal thickness on the IOP measurement (n=8 eyes/group). **(D):** Representative pictures of anterior OCT showing the corneal thickness and anterior chamber angle in the mice at 2-month after transplantation. *p<0.05, **p<0.01, ***p<0.001, **** p<0.0001.

149 **TMSCs Preserve the RGC Function of the Tg-MyocY437H Mice**

150 Preservation of RGC function is the goal for the treatment of POAG, so evaluating the
151 function of RGCs is critical in assessing the ability to reduce IOP for addressing
152 therapeutic effect of TMSCs on POAG. We used the Celeris to examine the pattern
153 electroretinogram (PERG), an optimal approach to detect RGC function (Figure 2).
154 WT mice showed the amplitude of P1 at 10.84 ± 0.86 μV at 6-month of age in the
155 PERG recording, while 40% of the RGC function lost in Tg-MyocY437H mice

156 calculated with the PERG (Tg, P1 = 6.56 ± 0.63 μV, p = 0.0001). With TMSC
157 transplantation, nearly 90% of the RGC function of the Tg-MyocY437H mice was
158 preserved (Tg-TMSC, P1 = 9.20 ± 0.45 μV, p = 0.19 vs WT, P1 = 10.84 ± 0.86 μV)
159 (Figure 2A-B).

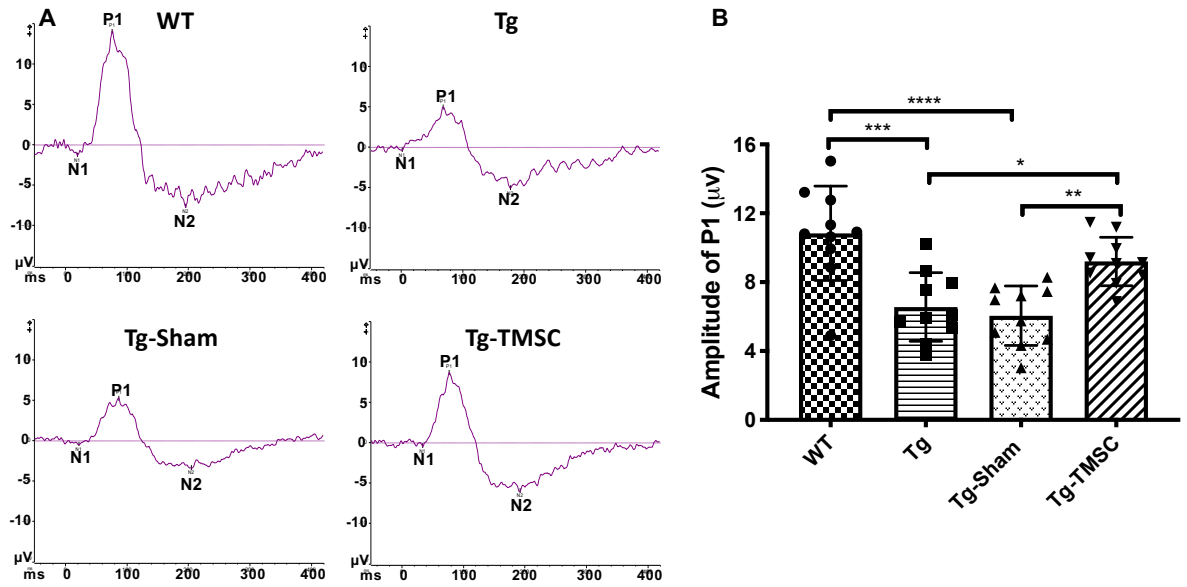

Figure 2. TMSCs preserve the function of retinal ganglion cells (RGCs) in Tg-Myoc Y437H mutation mice. The function of RGCs in the mice was evaluated by pattern electroretinogram (PERG). **(A):** Representative examples of PERG from different groups at 2-month after transplantation. (**B**): Bar graph of averaged P1 amplitude in PERG (n=10 eyes/group). *p<0.05, **p<0.01, ***p<0.001, ****p<0.0001. Abbreviations: WT: wildtype mice, Tg: Tg-MyocY437H mice, Tg-Sham: Tg mice with medium injection, Tg-TMSC: Tg mice with TMSC transplantation.

160 **TMSCs Increase the TM Cellularity in the Tg-MyocY437H Mice**

161 To further investigate mechanisms by which TMSCS reduced IOP and restored
162 outflow facility, we evaluated the TM cellular density in the mouse anterior segment
163 sections. Cellular density has been reported to be decreased due to apoptosis of TM
164 cells in Tg-MyocY437H mice(Zode et al., 2011). Collagen IV was used as a marker to
165 define the area of the TM tissue(Zhu et al., 2016). We combined the phase contrast
166 black-white image with collagen IV staining to accurately identify the TM region and
167 count the cells within the TM region. As shown in Figure 3A-B, the average number of
168 the cells in the TM region was 35.33 ± 2.50 cells/section in 6-month old WT mice
169 (n=10), while 42% and 51% of reduction of the TM cellularity was observed in the age-

170 matched Tg-MyocY437H mice (20.33 ± 1.11 cells/section, p <0.0001) and Tg-
171 MyocY437H mice with Sham injection (17.08 ± 1.18 cells/section, p <0.0001),
172 respectively. TMSC transplantation on Tg-MyocY437H mice increased the TM cell
173 number to 28.86 ± 1.46 cells/section (p = 0.0028 vs Tg mice, p <0.0001 vs Tg-Sham).

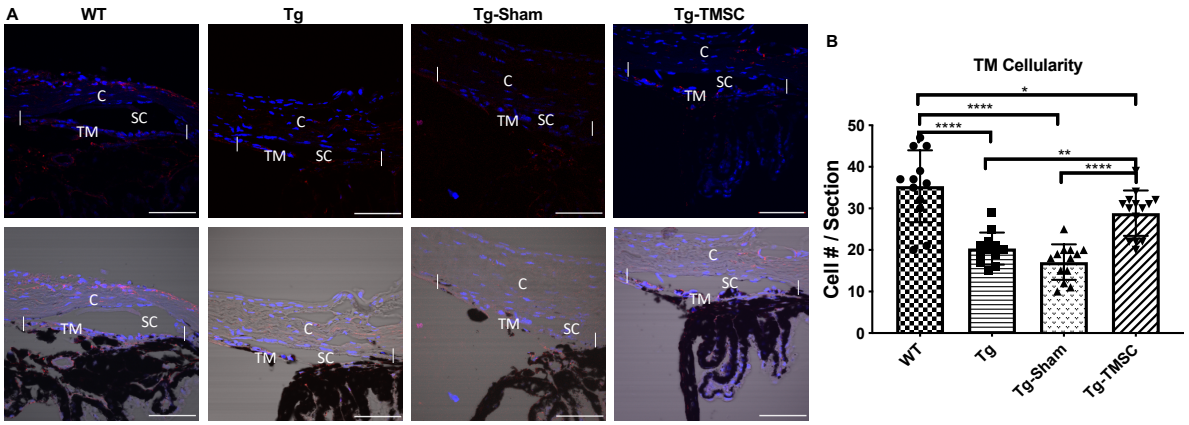

Figure 3. TMSCs increase TM cellularity in the Tg-MyocY437H (Tg) mice. (A): Evaluation of the cellular density in the mouse TM region. The section of anterior segment was immunostained with collagen IV (Red) and DAPI (blue). The TM region was determined by phase contrast image together with Collagen IV staining in the region between the two vertical lines. (**B**): The TM cellularity was averaged (n=12-14) and displayed as the number of cells in the TM region per section. Scale Bars, 50μm. *p<0.05, **p<0.01, **** p<0.0001. Abbreviations: **C:** cornea, **SC:** Schlemm's canal, **TM:** trabecular meshwork.

174 **TMSCs Facilitate Myocilin Secretion and Remodel Extracellular Matrix (ECM) in**
175 **Tg-MYOCY437H mice**

176 Characteristics of Tg-MyocY437H mice are the retention of misfolded Myoc protein in
177 the ER of the TM cells and reduced secretion of Myoc protein into aqueous
178 humor(Zode et al., 2011), which are associated with the upregulation of IOP in this
179 mouse model. Immunofluorescent staining on the paraffin sections showed that Myoc
180 protein was detectable in the TM region of WT mice, but expression was stronger in
181 the TM region of untreated and sham injected Tg-MyocY437H mice (Figure 4A).
182 However, Myoc expression in the TM region was reduced in the Tg-MyocY437H mice
183 receiving TMSC transplantation (Figure 4A). Western blotting on the limbal tissue
184 confirmed the immunostaining results and showed that TMSC transplantation reduced

185

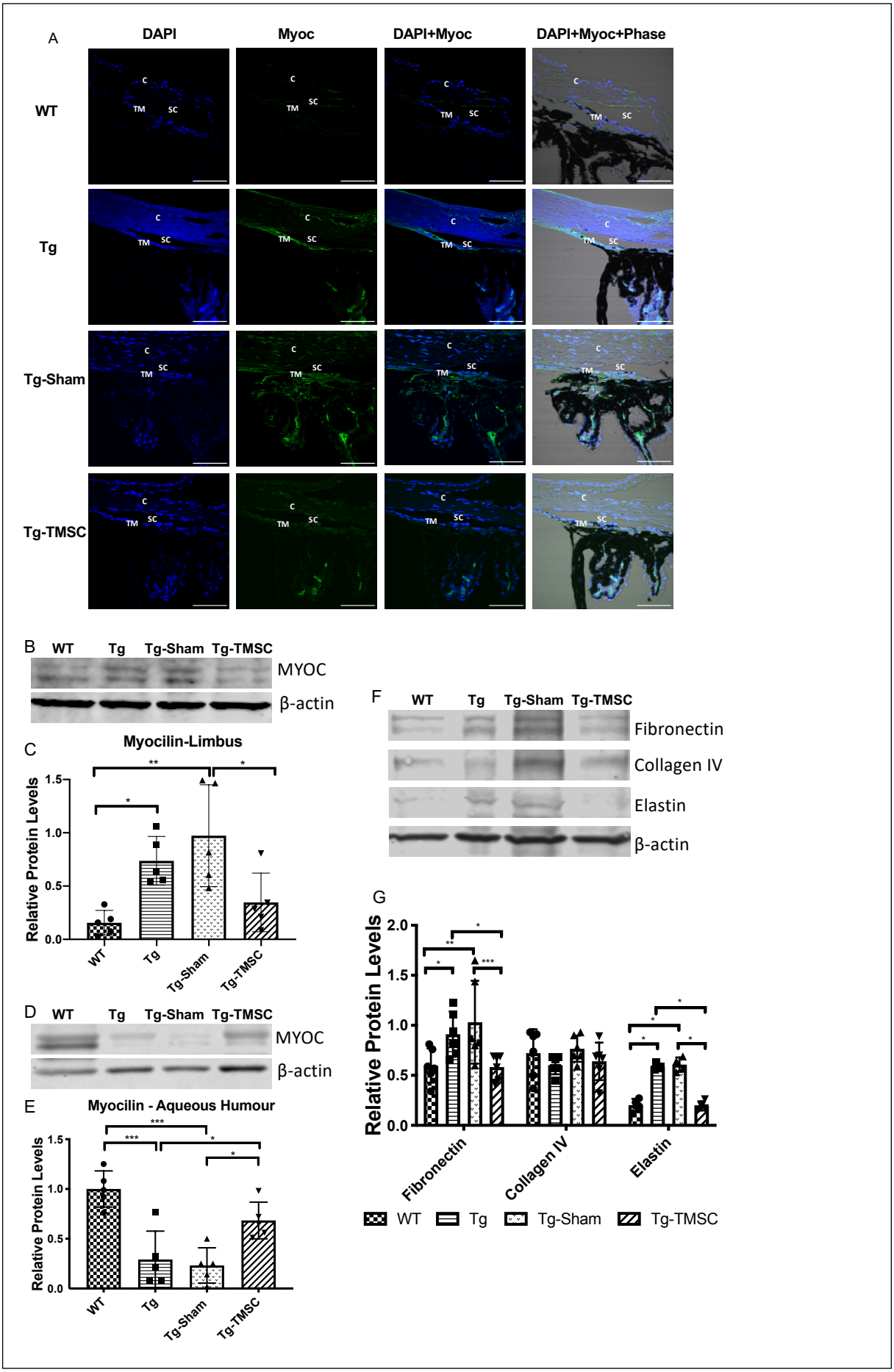
A
DAPI
Myoc
DAPI+Myoc
DAPI+Myoc+Phase
WT
Tg
Tg-Sham
Tg-TMSC
C
TM
SC
B
WT
Tg
Tg-Sham
Tg-TMSC
MYOC
β-actin
C
Myocilin-Limbus
Relative Protein Levels
1.5
1.0
0.5
0.0
WT
Tg
Tg-Sham
Tg-TMSC
D
WT
Tg
Tg-Sham
Tg-TMSC
MYOC
β-actin
E
Myocilin - Aqueous Humour
Relative Protein Levels
1.5
1.0
0.5
0.0
WT
Tg
Tg-Sham
Tg-TMSC
F
WT
Tg
Tg-Sham
Tg-TMSC
Fibronectin
Collagen IV
Elastin
β-actin
G
Relative Protein Levels
2.0
1.5
1.0
0.5
0.0
Fibronectin
Collagen IV
Elastin
WT
Tg
Tg-Sham
Tg-TMSC

Figure 4. TMSCs reduce the Myoc retention in the TM region, promote the Myoc secretion into the aqueous humor and reverse the extracellular matrix expression in the Tg-MyocY437H mice. **(A**): The expression of Myoc was evaluated in the mouse anterior segment by immunofluorescent staining. Accumulated Myoc was found in the TM and ciliary body in the Tg mice and Tg-sham mice. TMSC transplantation could resolve the aggregation of Myoc in the TM. **(B**): Representative bands indicating Myoc expression in the mouse limbal region by western blotting. **(C):** Relative Myoc protein levels in the limbus with β-actin as internal control (n=5). **(D):** Representative bands indicating Myoc expression in the mouse aqueous humor by western blotting. **(E):** Relative Myoc protein levels in the aqueous humor with β-actin as internal control (n=5). **(F):** Representative bands indicating the expression of ECM components fibronectin, collagen IV and elastin in the limbal region. **(G):** Relative ECM protein levels in the limbus with β-actin as internal control **(n=4-6).** Scale Bars, 50μm. *p<0.05, **p<0.01, ***p<0.001. Abbreviations: **C:** cornea, **SC:** Schlemm's canal, TM: trabecular meshwork.

186 contrast, very low levels of Myoc protein could be detected in the aqueous humor of
187 the Tg-MyocY437H and Tg-Sham mice, but Myoc protein was increased dramatically
188 in the aqueous humor of WT and in TMSC transplanted Tg-MyocY437H mice (Tg-
189 TMSCs) (Figure 4D-E). This indicates that TMSC transplantation can enhance the
190 secretion of Myoc protein into aqueous humor in the Tg-MyocY437H mice.

191 Abnormal deposition of ECM in the TM tissue is known to contribute to IOP elevation.
192 Indeed, increased levels of fibronectin and elastin were found in the limbus of the Tg-
193 MyocY437H and Tg-Sham mice, while collagen IV remained at the same level as that
194 seen in the WT mice (Figure 4F-G). However, TMSC transplantation downregulated
195 the expression of fibronectin and elastin in the TMSC treated Tg-MyocY437H mice to
196 the levels seen for WT mice (Figure 4F-G). This demonstrated that TMSCs could
197 change the expression pattern of ECM in the Tg-MyocY437H mice.

198

199 **The Effect of TMSCs on ER Stress in the TM of Tg-MyocY437H Mice**

200 To determine if TMSC transplantation could reduce ER stress seen in the TM of the
201 Tg-MyocY437H mice, immunoblotting was employed to detect the expression of ER
202 stress markers in mouse limbal tissue including the TM. Levels of ER stress markers
203 Grp 78 and Chop were significantly increased in the limbal tissue of Tg-MyocY437H
204 and Tg-Sham mice in comparison with the WT mice (Figure 5A-B). The expression of

205 Chop and Grp78 in the limbal tissue with TMSC injection was not significantly reduced
206 compared to the Tg-MyocY437H mice.
207 Further analyses by TEM revealed the ultrastructure of the TM tissue in Tg-
208 MyocY437H mice and Tg-Sham mice displayed enlarged ER lumen (Figure 5C,
209 Arrows). In contrast, TEM of the TM cells of Tg-MyocY437H mice receiving TMSC
210 transplantation indicated that increase in ER lumen seen in untreated and sham
211 treated Tg-MyocY437H mice was dramatically alleviated and more closely resembled
212 that of WT mice (Figure 5C, Arrows).

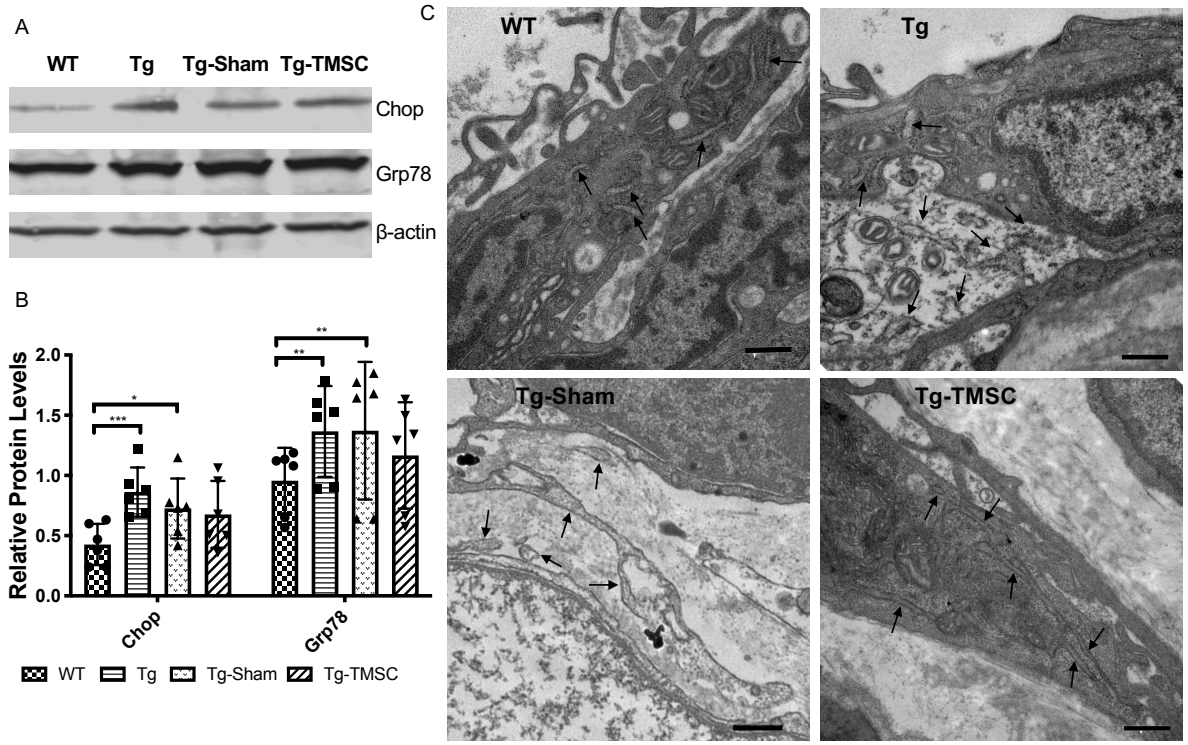

Figure 5. The effect of TMSCS on endoplasmic reticulum (ER) stress markers and ultrastructure of trabecular meshwork (TM) in the Tg-Myoc Y437H mice. (A): Representative bands showing the protein expression of ER stress markers, Grp78 and chop, in the mouse TM tissue by western blotting. **(B):** Relative protein levels with β-actin as internal control (n=6). **(C):** The ultrastructure of mouse TM region was examined by the transmission electron microscope (TEM) (40,000x). Black arrows point to the ER. Scale Bars, 500nm.). *p<0.05, **p<0.01, ***p<0.001.

213 **TMSCs Neither Stimulate Proliferation nor Reverse ER Stress of Mutant TM Cells**
214 ***in vitro***

215 To further explore the mechanisms behind regenerative effect of transplanted TMSCs
216 via increased TM cellularity, enhanced Myocilin secretion, remodeling of the TM ECM
217 and improvement of ER stress in the TM, we evaluated the effects of TMSCs on
218 transduced MyocY437H mutant TM cells in vitro. TM cells were transduced with
219 lentivirus which co-expressed GFP and Myoc with Y437H mutation. Transfected GFP-
220 positive cells were then sorted using flow cytometry and further passaged as a
221 predominantly GFP+ population of TM cells (Figure 6A). MyocY437H expressing GFP
222 positive TM cells were cultured alone, with TMSCs in the Transwell inserts or in direct
223 contact with TMSCs and further assessed. Proliferation of the transduced TM cells
224 was evaluated through analysis of incorporation rates of the EdU after 2-hour
225 incubation. Myoc mutant transduced TM cells showed 6.53 ± 1.19% EdU positivity,
226 while 6.06 ± 1.78% ($p = 0.8267$) and 6.51 ± 1.63% ($p = 0.9932$) of cells were EdU
227 positive when mutant TM cells were co-cultured with TMSCs in a Transwell insert or
228 in direct contact with TMSCs, respectively. This indicated that neither co-culturing nor
229 direct contact with TMSCs could stimulate proliferation of mutant TM cells (Figure 6B).
230 Next, we evaluated whether TMSCs could reduce ER stress in the Myoc mutant TM
231 cells. As shown in Figure 6C-D, high expression of Myoc and ER stress markers
232 (Grp78 and Chop) was detected in mutant TM cells compared with normal TM cells
233 and TM cells expressing GFP and the Myoc mutant protein. Co-culturing TM cells
234 with TMSCs in the Transwell insert could mimic the interactions seen in vivo between
235 homed TMSCs and TM cells. The co-culturing had little effect on reducing ER stress
236 or promoting Myoc secretion in the mutant TM cells. The expression of Grp78, Chop
237 and Myoc was similar to that without co-culturing.

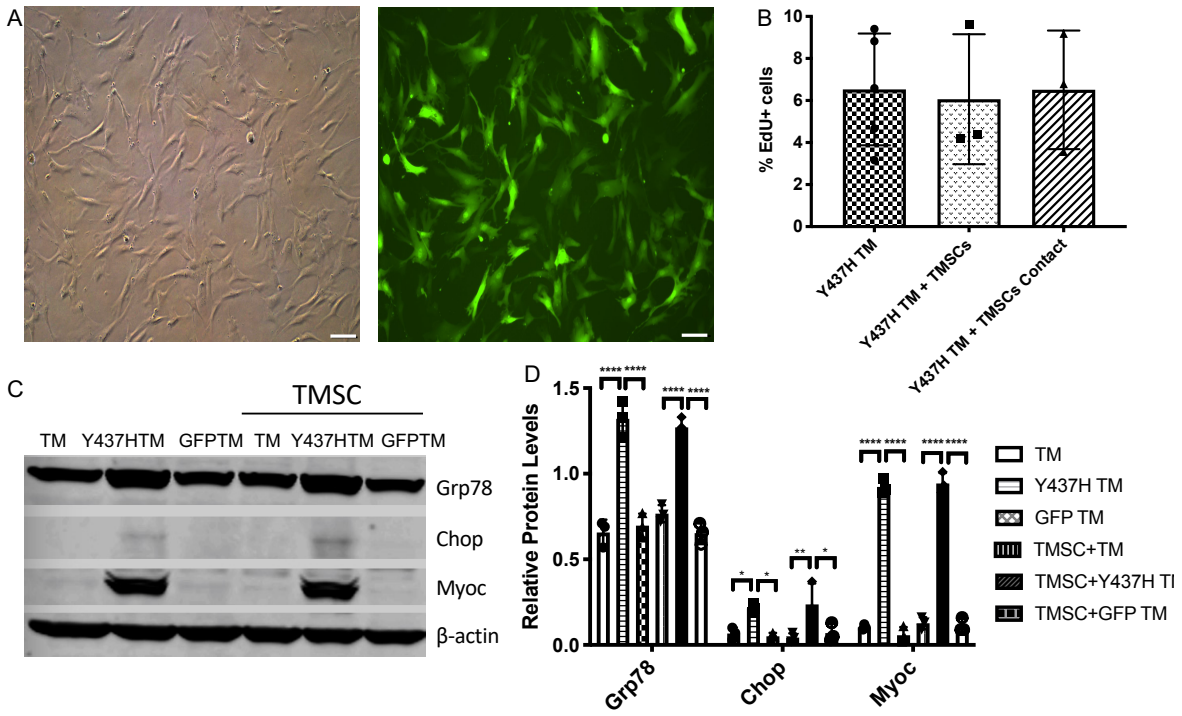

Figure 6. TMSCs could not reverse ER stress and stimulate proliferation in mutant TM cells in vitro. (A): The TM cells were transduced with recombinant lentivirus encoding GFP and mutant Myoc Y437H. The transduced GFP positive cells were sorted by Flow cytometry. After sorting, almost 100% TM cells expressed GFP (green) in the cytoplasm. **(B):** Flow cytometry analysis of EdU incorporation into cellular DNA of mutant TM cells with co-culture or direct contact with TMSCs for 4 days (n=3-5). **(C):** Representative western blotting bands showing the expression of ER stress markers and Myoc in the TM cells with or without TMSC co-culturing. **(D):** Relative protein levels with β-actin as internal control **(n=3).** Scale Bars, 100μm. *p<0.05, **p<0.01, **** p<0.0001. Abbreviations: **TM:** trabecular meshwork, **Y437H TM:** TM cells transduced with Myoc Y437H mutation, **GFP TM**: TM cells transduced with GFP only, **TMSC+xxx**: xxx cells co-cultured with TMSCs.

238 **TMSCs Differentiate into TM Cells Responsive to Dexamethasone and Gain**
239 **Phagocytic Function under the ER Stress Condition in vitro**

240 One of the mechanisms by which stem cells induce regeneration is differentiation into
241 cells of desired lineage to compensate for deficient cells in the injured tissue. We
242 previously reported that TMSCs could differentiate into TM cells and express TM
243 markers after homing to the TM tissues and being retained in normal mice(Du et al.,
244 2013) and in laser treated mice(Yun et al., 2018). However, the environment of the
245 Tg-MyocY437H mouse TM where TMSCs stayed is different. The TM tissue of Tg-
246 MyocY437H mice possesses ER stress with ECM changes(Kasetti, Phan, Millar, &
247 Zode, 2016). Understanding whether TMSCs can differentiate to TM cells under ER

248 stress condition could help to elucidate how TMSCs regulate IOP in the Tg-
249 MyocY437H mice. We co-cultured TMSCs together with the transduced Myoc mutant
250 TM cells. CHI3L1 expression (Figure 7A) was significantly increased in the TMSCs
251 after co-culturing (without contact) with normal TM cells (TM+TMSC) or with
252 MyocY437H mutant TM cells (Y437H TM+TMSC), in comparison with TMSCs without

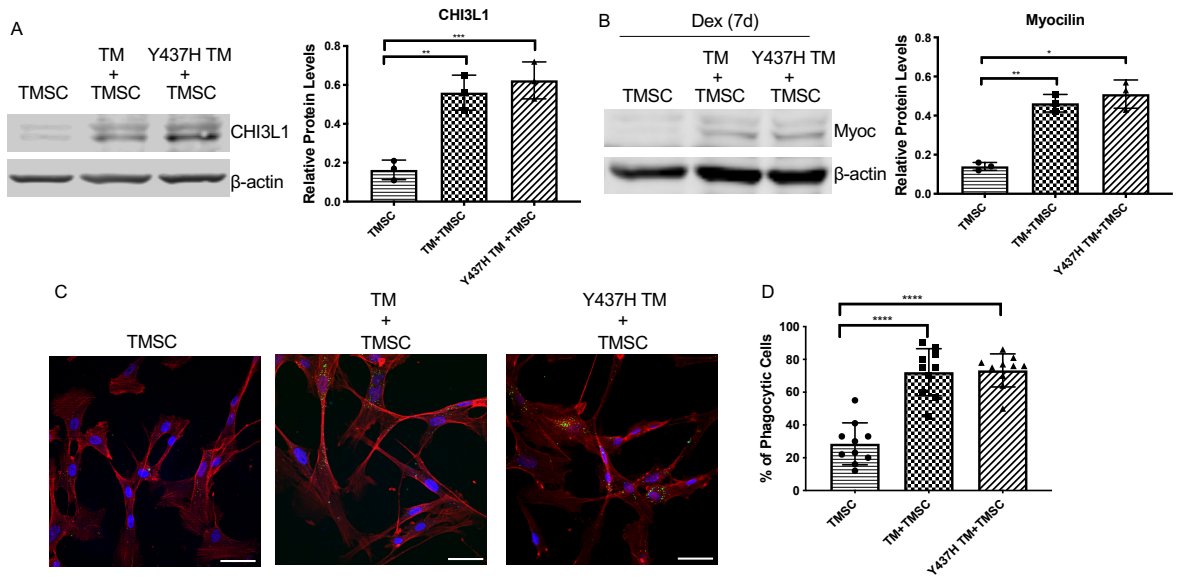

Figure 7. TMSCs differentiate into TM cells under ER stress environment. (A): The expression of CHI3L1 as one of the TM cell markers was upregulated in the TMSCs after 10 days of co-culturing with normal TM cells or Myoc Y437H mutant TM cells, n=3**. (B):** After co-culturing for 10 days, the co-cultured TM cells in the Transwell insert were removed, and TMSCs were further treated with dexamethasone (Dex) for 7 days. The levels of Myoc in these cells were detected by western blotting, n=3. (**C**): The mutant TM cells was used to mimic the ER stress environment that TMSCs would stay after transplantation into the Tg mice. After co-culturing of TMSCs with the TM cells in the Transwell insert for 10 days, the phagocytic ability of the TMSCs were evaluated by ingestion of bioparticles shown green in the cytoplasm. (**D**): Percentage of phagocytic cells averaged from 10 different views. Scale Bars, 50μm. **p<0.01, ***p<0.001，**** p<0.0001.

253 co-culture (TMSC). After another 7-day culture of the TMSCs in the presence of 100
254 nM dexamethasone, the expression of Myoc (Figure 7B) was significantly increased
255 in the TMSCs co-cultured with TM cells (TM+TMSC) or mutant TM cells (Y437H
256 TM+TMSC) while the Myoc expression was almost undetectable without co-culture
257 (TMSC). TMSCs co-cultured with normal and Myoc mutant TM cells gained the
258 phagocytic function indicated by ingesting fluorescent labeled bioparticles (Figure 7C-
259 D). Taken together, TMSCs were able to differentiate into TM cells responsive to

260 dexamethasone treatment and possessing the phagocytic function under ER stress
261 environment.

262 **TMSCs Had Upregulated Gene Expression Related to TM ECM Maintenance and**
263 **TM Regeneration.**

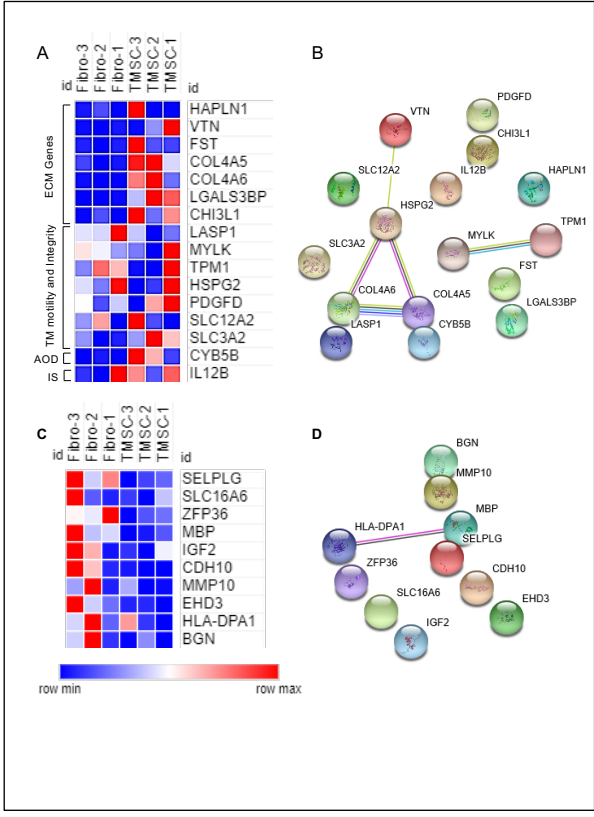

Figure 8. Transcriptome analysis of TM regeneration and POAG associated genes: A. Heatmap showing comparative expression of genes related to TM-extracellular matrix (ECM) in TMSCs (n=3) as compared to fibroblasts (n=3), AOD- Antioxidant Defense, IS- Immunosuppression. **B.** Interactome showing interaction network among TMSC upregulated ECM genes, **C.** Heatmap showing comparative expression of genes which are normally upregulated during Myocilin associated primary open angle glaucoma (Myoc-POAG), between TMSCs and fibroblasts, **D.** Interactome showing interaction network among fibroblast upregulated POAG genes. Results represent three individual TMSCs and fibroblasts obtained from different human donor tissues with at least 1.5-fold expression change without p value. Heatmaps were plotted using Morpheus.

264 We did RNA sequencing on three different strains of TMSCs and fibroblasts and
265 analyzed the transcriptome. We observed an upregulation of genes related to TM
266 ECM maintenance (HAPLN1, VTN, FST, COL4A5, COL4A6, LGALS3BP, CHI3L1),
267 TM integrity and motility (LASP1, MYLK, tPM1, HSPG2, PDGFD, SLC12A2, SLC3A2),
268 antioxidant defense (CYB5B), and immunosuppression (IL12B)(Liton et al., 2006) in
269 TMSCs as compared to fibroblasts (Figure 8A, Supplementary Table 1). Top three
270 upregulated pathways in TMSCs related to increased TM ECM interaction were (1)
271 Focal adhesion pathway including Vitronectin (VTN), Collagen Type IV Alpha 5 Chain
272 (COL4A5), Myosin light chain kinase (MYLK), Platelet Derived Growth Factor D
273 (PDGFD), and COL4A6; (2) PI3K-Akt signaling pathway including VTN, COL4A5,
274 PDGFD, and COL4A6; and (3) ECM-receptor interaction pathway including VTN,
275 COL4A5, Heparan sulfate proteoglycan core protein (HSPG2), and COL4A6 (Figure

276 8B, Supplementary Table 2). Genes related to Myocilin associated POAG (Liton et al.,
277 2006; Liu et al., 2013) such as P-selectin glycoprotein ligand-1 (SELPLG), Solute
278 Carrier Family 16 Member 6 (SLC16A6), Myelin basic protein (MBP), Insulin-like
279 growth factor 2 (IGF2) were upregulated in fibroblasts as compared to TMSCs (Figure
280 8C, Supplementary Table 3). We did not find correlation with any biological pathway
281 in these upregulated genes (Figure 8D).
282
283 **Discussion**
284 In this study we demonstrated that human TMSCs transplanted to the anterior
285 chamber of transgenic Myoc Y437H mutant mice alleviated many of the parameters
286 associated with glaucoma in a validated POAG mouse model. Specifically, TMSCs
287 reduced the IOP, increased the outflow facility and restored RGC function with
288 significantly improved pattern ERG. With TMSC transplantation, the TM cellularity in
289 the Tg-MyocY437H mice dramatically increased and the ECM components fibronectin
290 and elastin dramatically reduced in comparison with untreated and sham injected Tg-
291 MyocY437H mice. Although ER stress marker expression in the TM tissue was not
292 dramatically reduced after TMSC transplantation, the secreted Myoc into the aqueous
293 humor was significantly increased, while non-secreted Myoc in the TM tissue was
294 decreased to normal range compared to untreated and sham-treated Tg-MyocY437H
295 mice. In vitro co-culturing study indicated that TMSCs could differentiate into Dex-
296 responsive TM cells with phagocytic function in the presence of normal TM cells or
297 transduced TM cells with Myoc Y437H mutation. The TMSCs did not reverse ER
298 stress of cultured MyocY437H mutant TM cells in the co-culture platform. RNAseq
299 data analysis showing upregulation of genes related to TM regeneration including
300 maintenance of TM integrity, motility and ECM interaction in TMSCs as compared to
301 fibroblasts might explain that TMSCs induce regeneration in MyocY437H cells and Tg-
302 MyocY437H mice via modulation of ECM, increasing of TM integrity and motility, and
303 increasing the oxidative stress defense mechanism of TM cells. In contrast, fibroblasts

304 having inherent upregulation of POAG associated genes were unable to produce any
305 regenerative effect.
306 Our previous studies have shown that the response to ER stress inducers is
307 different between TMSCs and TM cells(Wang et al., 2019), and TMSCs can
308 differentiate into TM cells after homing in and retained in normal TM of WT mice(Du
309 et al., 2013) and in the laser-damaged TM for regeneration(Yun et al., 2018). However,
310 the microenvironment for the stem cells such as oxygen concentration, PH value,
311 osmotic pressure, proteases and cytokines, all affects the maintenance, survival and
312 regeneration properties of stem cells (Urban, 2002; Wuertz, Godburn, Neidlinger-
313 Wilke, Urban, & Iatridis, 2008). It was therefore crucial to confirm whether TMSCs
314 could convert to the TM cells in the Tg-MyocY437H mice with ER stress in the TM
315 tissue. We demonstrated that TMSCs could differentiate into TM cells expressing the
316 TM cell marker CHI3L1 (Du et al., 2012; Kelley et al., 2009; Wang et al., 2019) and
317 possessed phagocytic ability 10 days after co-culturing with the transduced Myoc
318 Y437H mutant TM cells. Phagocytic function of TM cells is responsible for ECM
319 turnover and maintenance of the outflow pathway by removing cell debris, which is
320 crucial for regulation of IOP. Moreover, the differentiated TMSCs were responsive to
321 dexamethasone treatment with increased expression of Myoc, one of the important
322 characteristics of TM cells(Keller et al., 2018). It indicates that TMSCs can
323 successfully differentiate to functional TM cells under ER stress condition.
324 The homeostasis of extracellular matrix in the TM tissue is known to be important
325 for maintaining IOP in the normal range(Vranka, Kelley, Acott, & Keller, 2015). Some
326 pathological stimuli can elevate IOP by breaking down ECM homeostasis, which
327 results in the excessive accumulation of ECM composition and insufficient degradation
328 of ECM in the TM tissue, thereby decreasing the outflow facility in this area(Acott &
329 Kelley, 2008). ER stress arising from mutant Myoc aggregates in the ER can destroy
330 assembly procedure of ECM proteins in the TM cells. The ECM components, such as
331 fibronectin, elastin and collagen IV were increased in the TM tissue due to abnormal
332 ER function and pathological cellular status in the Tg-MyocY437H mice(Kasetti et al.,

333 2016). Conversely, excessive ECM can aggravate ER stress in the TM cells, which
334 can form an negative feedback to keep the chronic ER stress existing in the Tg-
335 MyocY437H mice(Kasetti, Maddineni, Millar, Clark, & Zode, 2017). We found that
336 TMSC transplantation can reverse the expression of fibronectin and elastin to the
337 normal levels in the Tg-MyocY437H mouse TM tissue. Although the reduction of ER
338 stress marker expression after TMSC transplantation was not significant, the
339 expression level of Myoc reduced in the TM tissue and increased in the aqueous
340 humor, and a large number of cells displayed normal ultrastructure without swollen ER
341 in the TM region of the Tg-MyocY437H mice with TMSC transplantation. These
342 observations suggest that differentiated healthy TM cells from TMSCs replaced part
343 of the mutant TM cells and remodeled the ECM, improved the function of the diseased
344 TM tissue, which increased the outflow facility and reduced IOP.
345 Mesenchymal stem cells have been shown to reduce IOP in a laser-induced rat
346 glaucoma model(Manuguerra-Gagne et al., 2013). The activation of progenitor cells
347 in the ciliary body which can migrate and differentiate into TM cells in the damaged
348 tissue might be induced by laser photocoagulation or injected cells. Further research
349 is needed to elucidate whether TMSCs can recruit those progenitor cells to
350 synergistically repair tissues.
351 Loss of RGCs is the main reason of the impairment of visual field and loss of visual
352 acuity in POAG patients(Rolle, Dallorto, Briamonte, & Penna, 2014; Shoji et al., 2017).
353 Preserving the RGCs is as important as reducing IOP in treatment for glaucoma(Sena
354 & Lindsley, 2017; Stern et al., 2018). It is also a critical parameter to evaluate whether
355 stem cell-based therapy is suitable for the management of glaucoma(Pearson &
356 Martin, 2015). Elevation of IOP and subsequent loss of RGCs were observed in the
357 Tg-MyocY437H mice(Zode et al., 2011). Therefore, attention was paid to the
358 therapeutic effect of TMSCs on protection of RGC function. In this study, 90% of RGC
359 function was found to be saved after TMSC transplantation, while only 60% of RGC
360 function remained in the Tg-MyocY437H mice without treatment as compared to age-
361 matched WT mice. It indicated that TMSCs can prevent most of the RGCs from

362 degeneration resulted from IOP elevation. Nevertheless,10% of loss of RGC function
363 may be attributed to the delayed effect of TMSCs on reducing IOP in this glaucoma
364 model, in which IOP starts to elevate from 3 months of age while TMSCs were
365 transplanted at 4 months and the IOP reduced was observed at 5 months. Therefore,
366 whether earlier intervention can achieve more RGC survival needs further
367 investigation.
368 Our transcriptome analysis comparing TMSCs and fibroblasts indicates the activation
369 of different ECM modulation pathways like PI3K-Akt signaling pathway, Focal
370 adhesion pathway, ECM-receptor interaction pathway in TMSCs. These pathways are
371 involved in modifying ECM for regeneration(Villegas et al., 2013), associated with
372 stem cell migration and differentiation(Hu, Lu, Xu, Lyu, & Zhang, 2017), and cell
373 migration and adhesion(Bao et al., 2019). This discovery opens up future avenues to
374 be investigated which might improve our understanding of regeneration induced in
375 glaucoma by TMSCs.
376 **Conclusion**
377 Transplanted TMSCs can differentiate into TM cells that can repopulate the TM tissue,
378 remodel the TM ECM and restore the TM homeostasis to resolve outflow facility,
379 eventually reducing IOP and preserving RGC function in the Tg-MyocY437H mouse
380 model of POAG. These results open an important avenue of a novel stem cell-based
381 strategy to eventually treat human primary open-angle glaucoma.
382
383 **Materials and Methods**
384 **Animals**
385 Four-month old wildtype (WT) C57BL/6 mice were purchased from Jackson
386 Laboratory as the normal control, and Tg-MyocY437H mice were kindly gifted by Dr.
387 Gulab Zode (North Texas Eye Research Institute, Texas) and transferred to University
388 of Pittsburgh. All the experiments conducted on the animals were approved by the
389 University of Pittsburgh Institutional Animal Care and Use Committee and complied
390 with the ARVO Statement for the Use of Animals in Ophthalmic and Vision Research.

391 Mouse DNAs were isolated by biopsy from mouse ears for genotyping using the
392 primers: 5'-GACTAAGGCAAGAAAATGAGAATC-3' (Forward) and 5'-
393 CCTCTCCACTCCTGAGATAGC-3' (Reverse). Mice with PCR product at 249 bp were
394 regarded as carrying the Myoc mutation. The primer pair of 5'-
395 ACAAAGGCAGGGTCGAGAAGACAGG-3' (Forward) and 5'-
396 TTCCCACCTCTCTCTCCCCATGAGA-3' (Reverse) generated a 610 bp product that
397 was used to confirm the content of mouse DNA (Supplemental Figure 1).
398
399 **Intracameral Transplantation of TMSCs and IOP Measurement**
400 Human TMSCs were isolated and passaged as previous reported (Du et al., 2012;
401 Wang et al., 2019). Two TMSC strains from two different donors at passage 3 or 4
402 were used for cell injection. Mice were divided into four groups: Wildtype group (WT,
403 n=26), age-matched Tg-MyocY437H mice (Tg, n=26), Tg mice with intracameral
404 injection of the basal medium (Tg-Sham, n=26) and Tg mice with TMSC
405 transplantation (Tg-TMSC, n=26). Intracameral injection was following previous
406 published procedures (Du et al., 2013; Yun et al., 2018) with modifications. In brief,
407 mice at the age of 4 months were anesthetized with ketamine-xylazine. 3μl of medium
408 with 5×10^4 TMSCs or medium only (sham) were injected into the mouse anterior
409 chamber using a 33-gauge needle connected to a 25-μl Hamilton syringe. An I-
410 care tonometer was used to measure mouse IOP (TonoLab; Colonial Medical Supply,
411 Windham, NH). All IOP measurements were performed between 1:00 pm and 3:00
412 pm by at least two investigators with the one who measured IOP did not know what
413 groups the mice were (. IOP measurement before injection served as baseline and
414 was conducted at different time points at week 1, week 2**,** month 1 and month 2 after
415 transplantation.
416
417 **Measurement of Outflow Facility**
418 The procedure for measuring outflow facility was described previously(Lei, Overby,
419 Boussommier-Calleja, Stamer, & Ethier, 2011; Yun et al., 2018). All the outflow

420 measurements on mouse eyes were finished within 6 hours after enucleation. Eyes
421 were irrigated with phosphate buffer saline (PBS) at constant pressures of 4, 8, 15,
422 and 25 mmHg and outflow was recorded at least 15 minutes at each pressure after
423 the pressure was stable. Twelve eyes from each group were then perfused. Outflow
424 facility (μL/min/mmHg) was calculated using the Goldmann equation (Lei et al., 2011).
425 Data were excluded when R^2 equaled or was less than 0.95 and accepted data from
426 six eyes per group were analyzed and averaged.
427

428 **Transmission Electron Microscopy**

429 Transmission electron microscopy (TEM) was used to evaluate the ultrastructure of
430 the TM as described previously (Yun et al., 2014). After removing the iris, the limbus
431 tissues (n=3) from each group were fixed in Karnovsky's fixative. Subsequently, the
432 tissues were dehydrated and embedded in Epon and 65 nm Ultrathin sections were
433 cut, stained with uranyl acetate (Electron Microscopy Sciences) and Reynold's lead
434 citrate (Fisher). Sections were photographed at 80 kV on a Jeol 1011 TEM for analysis.
435

436 **Immunostaining and Counting of TM Cellularity**

437 The mouse eyes were fixed in 4% formaldehyde overnight and embedded in paraffin.
438 After dewaxing, rehydration, Heat-Induced Epitope Retrieval (HIER) and blocking with
439 10% normal serum, sections were incubated with primary antibodies to myocilin
440 (Novus Biologicals) and collagen IV(Abcam) overnight at 4°C. After 3 washes with
441 PBS, corresponding fluorescent secondary antibodies and 4′,6-diamidino-2-
442 phenylindole (DAPI) were applied to the sections for 1 hour. After 5 washes, slides
443 were mounted and imaged using a confocal microscope (Olympus IX81) and analyzed
444 on FV10-ASW4.2 Viewer (Olympus). For measuring TM cellularity, primary antibody
445 against collagen IV, together with images from phase contrast, were used to define
446 the TM region in the sections. Cell nuclei stained with DAPI within the TM region were
447 counted under FV10-ASW4.2 Viewer. Images of at least 10 fields per group were
448 photographed, and the number of cell nuclei per field was counted and averaged.

449

450 **Phagocytosis Assay**

451 Cells were incubated with opsonized Alexa 546-conjugated S. aureus bioparticles
452 (ThermoFisher) at a ratio of 20 bioparticles per cell at 37°C for 1 hour. After incubation,
453 the cells were washed with PBS, trypsinized and transferred to another 6-well plated
454 with coverslips at the bottom to get rid of any noningested bioparticles. After
455 attachment, cells were fixed with 4% paraformaldehyde, permeabilized with 0.5%
456 Triton X-100, and incubated with phalloidin conjugated with AlexFluor-647 and DAPI.
457 Cellular phagocytosis of bioparticles which were ingested by the cells was observed
458 within the cytoplasm and photographed under a confocal microscope (Olympus). At
459 least 10 individual views per condition were counted and averaged. The phagocytic
460 ability was calculated as following:

461 $$\%\ of\ Phagocytic\ cells = \frac{Number\ of\ phagocytosed\ cells/field}{Total\ Cell\ Number/field} \times 100$$

462

463 **Construction of Recombinant Lentivirus $^{\text{Myoc Y437H/GFP}}$**

464 Recombinant Lentiviral Vector encoding Myoc Y437H was constructed from
465 plasmids pLent$^{\text{CMV-GFP}}$(Addgene 17448)(Campeau et al., 2009), p$^{\text{CAGIG2}}$ (Addgene
466 111159) (Matsuda & Cepko, 2004) and pcDNA3$^{\text{Myoc Y437H}}$ (Zadoo, Nguyen, Zode, &
467 Hulleman, 2016). Briefly, pLenti $^{\text{CMV-GFP-Puro}}$ was digested with BamHI and SalI (NEB)
468 to remove GFP cassette and served as the vector backbone, which was utilized to
469 generate lentivirus encoding plasmid (pLenti $^{\text{CMV-IRES-GFP}}$) by insertion of IRES-EGFP
470 cassette (obtained from p$^{\text{CAGIG2}}$) into it. The cDNA sequence containing Tyr437His
471 mutation was amplified from pcDNA3$^{\text{Myoc Y437H}}$ by using the primers: Forward 5'-
472 ACACCGACTCTAGAGATGAGGTTCTTCTGTGCACGT-3' and Reverse 5 '-
473 GGCGACCGGTGGATCTCA CATCTTGGAGAGCTTGATG- 3'. It was subsequently
474 cloned into BamHI site in the pLenti $^{\text{CMV-IRES-GFP}}$ by In-Fusion cloning kit (Clontech,
475 639649) to generate lentiviral packaging plasmids(pLenti$^{\text{CMV-Y437H-IRES-GFP}}$), which were
476 co-transfected with ViraPower^{R} Lentiviral Packaging Mix (Invitrogen) in to 293T cells
477 using Lipofectamine 3000 Reagent (Invitrogen, L3000015) for Lentivirus assembly.

478 The supernatant of transfected cells taken at day 5 was then concentrated with Lenti-
479 X Concentrator (TakKaRa, 631232) for the collection of recombinant lentivirus
480 encoding the mutant myocilin (Supplemental Figure 2).
481
482 **Cell Culture and Lentivirus Transduction**
483 The donor human corneas containing TM tissue were obtained from the Center for
484 Organ Recovery and Education (Pittsburgh, PA) and used for isolation of TM cells and
485 TMSCs. The cells were cultured and passaged as previously reported (Du et al., 2012;
486 Wang et al., 2019). Human TM cells were cultured in Dulbecco's modified Eagle's
487 medium (DMEM)/F12 with 10% fetal bovine serum (FBS). Human TMSCs were
488 cultured in Opti-MEM (Invitrogen) with 5% FBS and a variety of supplements(Du et al.,
489 2012).The TMSCs and TM cells at passages 3-4 were used for the experiments in this
490 study.
491 **Lentivirus transduction:** Primary TM cells at passage 3 and 70% confluence were
492 transduced with lentivirus encoding both mutant Myoc and GFP protein or GFP alone
493 as a control at a multiplicity of infection (MOI) 3. Polybrene was used at 6 μg/ml to
494 increase transduction efficiency. GFP positive cells were sorted through Flow
495 cytometry (BD Biosciences, San Jose, CA) 3 days after transduction and passaged
496 for the following studies.
497 **Co-culture of TMSCs and TM Cells:** For analyzing the effect of TMSCs on reversing
498 ER stress and relieving accumulation of mutant Myoc in transduced TM cells, 5×10^4
499 TMSCs were seeded in the upper chamber of 6-well Corning Transwell inserts, while
500 5×10^4 normal TM cells or transduced TM cells with MyocY437H mutation were
501 maintained at the bottom of the plates. To determine whether TMSCs could stimulate
502 proliferation of mutant TM cells, 5×10^4 TMSCs were plated directly on pre-plated 5×10^4
503 Myoc mutant TM cells or TMSCs were in Transwell inserts as just described and cells
504 were cocultured for 4 days. To determine if TMSCs could differentiate into TM cells
505 under ER stress environment, 5×10^4 mutant MyocY437H TM cells in the inserts were
506 cocultured with 5×10^4 TMSCs for 10 days. Then, the upper inserts containing mutant

507 TM cells were removed, the TMSCs in the bottom compartment were utilized for
508 phagocytosis assay or further cultured with dexamethasone (100 nM) for another 7
509 days.
510
511 **EdU Incorporation and Flow Cytometry Analysis**
512 To determine whether TMSCs influence the proliferation of mutant TM cells, the
513 MyocY437H TM cells were cultured alone, with TMSCs in the Transwell inserts, or in
514 direct contact with TMSCs. When cells reached 70% confluence, EdU was added into
515 the culture medium to reach 10 μM concentration and incubated for 2 hours. The cells
516 were then trypsinized, fixed with 4% paraformaldehyde, permeabilized with 0.5% of
517 Triton X-100 and blocked with 1% bovine serum albumin (BSA). Subsequently, a
518 cocktail containing sodium ascorbate (10 mM), azide-fluor 545 (8 μM) and copper
519 sulfate (1 mM) was added and incubated for 10 minutes. Cells not undergoing the
520 staining procedure, and cells incubating with azide-fluor 545 only were used as
521 controls. Cell samples were run on the flow cytometer to gate both GFP+ mutant TM
522 cells and EdU+ cells. The analysis was done using FlowJo_V10 software (FlowJo,
523 Ashland, OR) and the percentage of EdU+ cells was counted as the number of
524 GFP+EdU+ cells divided by GFP+ cells x 100. Each group was replicated at least
525 three times.
526
527 **Western Blotting Analysis**
528 Cultured cells, aqueous humor and mouse limbus tissue were lysed with RIPA buffer
529 (Santa Cruz Biotechnology). BCA Protein Assay Kit (Pierce Biotechnology) was
530 utilized for evaluating the concentration of proteins. 30 μg total protein was loaded in
531 each well and electrophoresed on the sodium dodecyl sulfate–polyacrylamide gel
532 (ThermoFisher) and transferred to the PVDF membrane. After blocking in the blocking
533 buffer, the membrane was incubated overnight with following primary antibodies
534 accordingly, anti-CHI3L1, anti-Myoc, anti-elastin (Novus), anti-Grp78, anti-fibronectin
535 and anti-collagenIV (Abcam). After washing with 0.1% Tween 20 in Tris-buffered

536 saline for three times, it was incubated with secondary antibodies (IRDye 680LT and
537 IRDye 800CW, LI-COR Biosciences). Fluorescent signals were captured on an
538 infrared imager (Odyssey; LI-COR Biosciences). ImageJ was used for the analysis of
539 protein expression. Each study was repeated three times.
540
541 **Anterior Segment Optical Coherence Tomography (OCT)**
542 For evaluation of central corneal thickness and peripheral anterior synechia, an
543 anterior segment optical coherence tomography (OCT; Visante OCT MODEL 1000;
544 Carl Zeiss Meditec, Dublin, CA) was used. Eight eyes of each group were examined
545 by determining quadrant-scans along four axes (0°–180°, 45°–225°, 90°–270°, and
546 135°–315°) to ensure scanning through the central cornea and data along the 0° to
547 180° axis were used for analysis.
548
549 **Pattern Electroretinography (PERG)**
550 PERG was performed on the Celeris apparatus (Diagnosys LLC, Lowell, MA) to
551 evaluate the RGC function. Mice (n=10 eyes for each group) were anesthetized with
552 intraperitoneal injections of the mixture of ketamine and xylazine. The murine pupil
553 was dilated with 0.5% tropicamide and 2.5% phenylephrine eye drops. A circular
554 electrode centered on the cornea was placed in a plane perpendicular to the visual
555 axis. Pattern stimuli consisted of horizontal bars of variable spatial frequencies and
556 contrast that alternate at different temporal frequency. The parameters for PERG
557 amplitude were spatial frequency 0.155 cycles/degree, temporal frequency 2.1
558 reversals/sec, contrast 100% and substantial averaging (600-1800 sweeps). The
559 amplitude of P1 was used to analyze the function of RGCs.
560
561 **RNA sequencing:**
562 Three strains of cultured TMSCs and fibroblasts were lysed in RLT buffer (Qiagen).
563 RNA isolation was performed using RNeasy mini kit (Qiagen) as per manufacturer's
564 instructions. RNA pellet was treated with Ambion™ RNase-free DNase in 10X DNase

565 1 buffer (Invitrogen). Final RNA pellet was dissolved in RNase-free diethyl
566 pyrocarbonate (DEPC) water and sent to GENEWIZ, LLC. (South Plainfield, NJ, USA)
567 for RNA sequencing. Heatmaps were generated using morpheus, software from Broad
568 institute (https://software.broadinstitute.org/morpheus/). Interactome networks were
569 generated using STRING v11 (Szklarczyk et al., 2019).
570

571 **Statistical Analysis**

572 The results were expressed as mean ± standard deviation (SD). The statistical
573 differences were analyzed by two-way ANOVA (for Fig1A, 4G, 5B, 6D) or one-way
574 ANOVA (for all others) followed by Tukey's multiple comparisons test in GraphPad
575 Prism version 8. $p < 0.05$ was considered statistically significance.
576

577 **Acknowledgments**

578 The work was supported by NIH grants EY025643 (YD), P30-EY008098, Research to
579 Prevent Blindness; and Eye and Ear Foundation (Pittsburgh, PA). The authors thank
580 Kira Lathrop for assisting with confocal microscopy, Nancy Zurowski with Flow
581 Cytometry, Katherine Davoli for paraffin sectioning, and Ming Sun for TEM sectioning.

582 **AUTHOR CONTRIBUTIONS**

583 S.X.: conception and design, collection of data, data analysis and interpretation,
584 manuscript writing, final approval of manuscript; S.T., A.K., S.T., E.E.T.: collection of
585 data, data analysis and interpretation, final approval of manuscript; E.Y.: collection of
586 data, administrative support, final approval of manuscript; P.R.K., data analysis and
587 interpretation, final approval of manuscript; X.X.: conception and design, data analysis
588 and interpretation, final approval of manuscript; Y.D.: conception and design, financial
589 support, administrative support, collection of data, data analysis and interpretation,
590 manuscript writing, final approval of manuscript.
591

592 **Data Availability Statement**

593 All the supporting data have been submitted.

References

Abu-Hassan, D. W., Li, X., Ryan, E. I., Acott, T. S., & Kelley, M. J. (2015). Induced pluripotent stem cells restore function in a human cell loss model of open-angle glaucoma. *Stem Cells, 33*(3), 751-761. doi:10.1002/stem.1885

Acott, T. S., & Kelley, M. J. (2008). Extracellular matrix in the trabecular meshwork. *Exp Eye Res, 86*(4), 543-561. doi:10.1016/j.exer.2008.01.013

Alvarado, J., Murphy, C., & Juster, R. (1984). Trabecular meshwork cellularity in primary open-angle glaucoma and nonglaucomatous normals. *Ophthalmology, 91*(6), 564-579. doi:10.1016/s0161-6420(84)34248-8

Alvarado, J., Murphy, C., Polansky, J., & Juster, R. (1981). Age-related changes in trabecular meshwork cellularity. *Invest Ophthalmol Vis Sci, 21*(5), 714-727.

Bao, Y., Wang, L., Shi, L., Yun, F., Liu, X., Chen, Y., . . . Jia, Y. (2019). Transcriptome profiling revealed multiple genes and ECM-receptor interaction pathways that may be associated with breast cancer. *Cell Mol Biol Lett, 24*, 38. doi:10.1186/s11658-019-0162-0

Braunger, B. M., Ademoglu, B., Koschade, S. E., Fuchshofer, R., Gabelt, B. T., Kiland, J. A., . . . Tamm, E. R. (2014). Identification of adult stem cells in Schwalbe's line region of the primate eye. *Invest Ophthalmol Vis Sci, 55*(11), 7499-7507. doi:10.1167/iovs.14-14872

Broman, A. T., Quigley, H. A., West, S. K., Katz, J., Munoz, B., Bandeen-Roche, K., . . . Foster, P. J. (2008). Estimating the rate of progressive visual field damage in those with open-angle glaucoma, from cross-sectional data. *Invest Ophthalmol Vis Sci, 49*(1), 66-76. doi:10.1167/iovs.07-0866

Buller, C., Johnson, D. H., & Tschumper, R. C. (1990). Human trabecular meshwork phagocytosis. Observations in an organ culture system. *Invest Ophthalmol Vis Sci, 31*(10), 2156-2163.

Campeau, E., Ruhl, V. E., Rodier, F., Smith, C. L., Rahmberg, B. L., Fuss, J. O., . . . Kaufman, P. D. (2009). A versatile viral system for expression and depletion of proteins in mammalian cells. *PLoS One, 4*(8), e6529. doi:10.1371/journal.pone.0006529

Du, Y., Roh, D. S., Mann, M. M., Funderburgh, M. L., Funderburgh, J. L., & Schuman, J. S. (2012). Multipotent stem cells from trabecular meshwork become phagocytic TM cells. *Invest Ophthalmol Vis Sci, 53*(3), 1566-1575. doi:10.1167/iovs.11-9134

Du, Y., Yun, H., Yang, E., & Schuman, J. S. (2013). Stem cells from trabecular meshwork home to TM tissue in vivo. *Invest Ophthalmol Vis Sci, 54*(2), 1450-1459. doi:10.1167/iovs.12-11056

Fingert, J. H., Stone, E. M., Sheffield, V. C., & Alward, W. L. (2002). Myocilin glaucoma. *Surv Ophthalmol, 47*(6), 547-561.

Heijl, A., Leske, M. C., Bengtsson, B., Hyman, L., Bengtsson, B., Hussein, M., & Early Manifest Glaucoma Trial, G. (2002). Reduction of intraocular pressure and glaucoma progression: results from the Early Manifest Glaucoma Trial. *Arch Ophthalmol, 120*(10), 1268-1279. doi:10.1001/archopht.120.10.1268

636 Hu, Y., Lu, J., Xu, X., Lyu, J., & Zhang, H. (2017). Regulation of focal adhesion turnover in
637 SDF-1alpha-stimulated migration of mesenchymal stem cells in neural differentiation.
638 *Sci Rep, 7*(1), 10013. doi:10.1038/s41598-017-09736-7
639 Janssen, S. F., Gorgels, T. G., Ramdas, W. D., Klaver, C. C., van Duijn, C. M., Jansonius, N.
640 M., & Bergen, A. A. (2013). The vast complexity of primary open angle glaucoma:
641 disease genes, risks, molecular mechanisms and pathobiology. *Prog Retin Eye Res,*
642 *37*, 31-67. doi:10.1016/j.preteyeres.2013.09.001
643 Kasetti, R. B., Maddineni, P., Millar, J. C., Clark, A. F., & Zode, G. S. (2017). Increased
644 synthesis and deposition of extracellular matrix proteins leads to endoplasmic
645 reticulum stress in the trabecular meshwork. *Sci Rep, 7*(1), 14951.
646 doi:10.1038/s41598-017-14938-0
647 Kasetti, R. B., Phan, T. N., Millar, J. C., & Zode, G. S. (2016). Expression of Mutant
648 Myocilin Induces Abnormal Intracellular Accumulation of Selected Extracellular
649 Matrix Proteins in the Trabecular Meshwork. *Invest Ophthalmol Vis Sci, 57*(14),
650 6058-6069. doi:10.1167/iovs.16-19610
651 Keller, K. E., Aga, M., Bradley, J. M., Kelley, M. J., & Acott, T. S. (2009). Extracellular
652 matrix turnover and outflow resistance. *Exp Eye Res, 88*(4), 676-682.
653 doi:10.1016/j.exer.2008.11.023
654 Keller, K. E., Bhattacharya, S. K., Borras, T., Brunner, T. M., Chansangpetch, S., Clark, A.
655 F., . . . Stamer, W. D. (2018). Consensus recommendations for trabecular meshwork
656 cell isolation, characterization and culture. *Exp Eye Res, 171*, 164-173.
657 doi:10.1016/j.exer.2018.03.001
658 Kelley, M. J., Rose, A. Y., Keller, K. E., Hessle, H., Samples, J. R., & Acott, T. S. (2009).
659 Stem cells in the trabecular meshwork: present and future promises. *Exp Eye Res,*
660 *88*(4), 747-751. doi:10.1016/j.exer.2008.10.024
661 Kumar, A., Xu, Y., & Du, Y. (2020). Stem Cells from Human Trabecular Meshwork Hold
662 the Potential to Develop into Ocular and Non-Ocular Lineages After Long-Term
663 Storage. *Stem Cells Dev, 29*(1), 49-61. doi:10.1089/scd.2019.0169
664 Lei, Y., Overby, D. R., Boussommier-Calleja, A., Stamer, W. D., & Ethier, C. R. (2011).
665 Outflow physiology of the mouse eye: pressure dependence and washout. *Invest*
666 *Ophthalmol Vis Sci, 52*(3), 1865-1871. doi:10.1167/iovs.10-6019
667 Liesenborghs, I., Eijssen, L. M. T., Kutmon, M., Gorgels, T., Evelo, C. T., Beckers, H. J.
668 M., . . . Schouten, J. (2019). Comprehensive bioinformatics analysis of trabecular
669 meshwork gene expression data to unravel the molecular pathogenesis of primary
670 open-angle glaucoma. *Acta Ophthalmol*. doi:10.1111/aos.14154
671 Liton, P. B., Luna, C., Challa, P., Epstein, D. L., & Gonzalez, P. (2006). Genome-wide
672 expression profile of human trabecular meshwork cultured cells, nonglaucomatous
673 and primary open angle glaucoma tissue. *Mol Vis, 12*, 774-790.
674 Liu, Y., Allingham, R. R., Qin, X., Layfield, D., Dellinger, A. E., Gibson, J., . . . Hauser, M.
675 A. (2013). Gene expression profile in human trabecular meshwork from patients with
676 primary open-angle glaucoma. *Invest Ophthalmol Vis Sci, 54*(9), 6382-6389.
677 doi:10.1167/iovs.13-12128
678 Manuguerra-Gagne, R., Boulos, P. R., Ammar, A., Leblond, F. A., Krosl, G., Pichette,
679 V., . . . Roy, D. C. (2013). Transplantation of mesenchymal stem cells promotes tissue

680 regeneration in a glaucoma model through laser-induced paracrine factor secretion
681 and progenitor cell recruitment. *Stem Cells, 31*(6), 1136-1148. doi:10.1002/stem.1364
682 Matsuda, T., & Cepko, C. L. (2004). Electroporation and RNA interference in the rodent
683 retina in vivo and in vitro. *Proc Natl Acad Sci U S A, 101*(1), 16-22.
684 doi:10.1073/pnas.2235688100
685 Pearson, C., & Martin, K. (2015). Stem cell approaches to glaucoma: from aqueous outflow
686 modulation to retinal neuroprotection. *Prog Brain Res, 220*, 241-256.
687 doi:10.1016/bs.pbr.2015.04.005
688 Peters, J. C., Bhattacharya, S., Clark, A. F., & Zode, G. S. (2015). Increased Endoplasmic
689 Reticulum Stress in Human Glaucomatous Trabecular Meshwork Cells and Tissues.
690 *Invest Ophthalmol Vis Sci, 56*(6), 3860-3868. doi:10.1167/iovs.14-16220
691 Quigley, H. A., & Broman, A. T. (2006). The number of people with glaucoma worldwide in
692 2010 and 2020. *Br J Ophthalmol, 90*(3), 262-267. doi:10.1136/bjo.2005.081224
693 Raviola, G. (1982). Schwalbe line's cells: a new cell type in the trabecular meshwork of
694 Macaca mulatta. *Invest Ophthalmol Vis Sci, 22*(1), 45-56.
695 Rolle, T., Dallorto, L., Briamonte, C., & Penna, R. R. (2014). Retinal nerve fibre layer and
696 macular thickness analysis with Fourier domain optical coherence tomography in
697 subjects with a positive family history for primary open angle glaucoma. *Br J*
698 *Ophthalmol, 98*(9), 1240-1244. doi:10.1136/bjophthalmol-2013-304519
699 Sena, D. F., & Lindsley, K. (2017). Neuroprotection for treatment of glaucoma in adults.
700 *Cochrane Database Syst Rev, 1*, CD006539. doi:10.1002/14651858.CD006539.pub4
701 Shoji, T., Zangwill, L. M., Akagi, T., Saunders, L. J., Yarmohammadi, A., Manalastas, P. I.
702 C., . . . Weinreb, R. N. (2017). Progressive Macula Vessel Density Loss in Primary
703 Open-Angle Glaucoma: A Longitudinal Study. *Am J Ophthalmol, 182*, 107-117.
704 doi:10.1016/j.ajo.2017.07.011
705 Stern, J. H., Tian, Y., Funderburgh, J., Pellegrini, G., Zhang, K., Goldberg, J. L., . . . Temple,
706 S. (2018). Regenerating Eye Tissues to Preserve and Restore Vision. *Cell Stem Cell,*
707 *22*(6), 834-849. doi:10.1016/j.stem.2018.05.013
708 Szklarczyk, D., Gable, A. L., Lyon, D., Junge, A., Wyder, S., Huerta-Cepas, J., . . . Mering,
709 C. V. (2019). STRING v11: protein-protein association networks with increased
710 coverage, supporting functional discovery in genome-wide experimental datasets.
711 *Nucleic Acids Res, 47*(D1), D607-D613. doi:10.1093/nar/gky1131
712 Tamm, E. R. (2002). Myocilin and glaucoma: facts and ideas. *Prog Retin Eye Res, 21*(4),
713 395-428.
714 Urban, J. P. (2002). The role of the physicochemical environment in determining disc cell
715 behaviour. *Biochem Soc Trans, 30*(Pt 6), 858-864. doi:10.1042/bst0300858
716 Villegas, S. N., Rothova, M., Barrios-Llerena, M. E., Pulina, M., Hadjantonakis, A. K., Le
717 Bihan, T., . . . Brickman, J. M. (2013). PI3K/Akt1 signalling specifies foregut
718 precursors by generating regionalized extra-cellular matrix. *Elife, 2*, e00806.
719 doi:10.7554/eLife.00806
720 Vranka, J. A., Kelley, M. J., Acott, T. S., & Keller, K. E. (2015). Extracellular matrix in the
721 trabecular meshwork: intraocular pressure regulation and dysregulation in glaucoma.
722 *Exp Eye Res, 133*, 112-125. doi:10.1016/j.exer.2014.07.014

723 Wang, Y., Osakue, D., Yang, E., Zhou, Y., Gong, H., Xia, X., & Du, Y. (2019). Endoplasmic
724 Reticulum Stress Response of Trabecular Meshwork Stem Cells and Trabecular
725 Meshwork Cells and Protective Effects of Activated PERK Pathway. *Invest*
726 *Ophthalmol Vis Sci, 60*(1), 265-273. doi:10.1167/iovs.18-25477
727 Wuertz, K., Godburn, K., Neidlinger-Wilke, C., Urban, J., & Iatridis, J. C. (2008). Behavior
728 of mesenchymal stem cells in the chemical microenvironment of the intervertebral
729 disc. *Spine (Phila Pa 1976), 33*(17), 1843-1849. doi:10.1097/BRS.0b013e31817b8f53
730 Yun, H., Lathrop, K. L., Yang, E., Sun, M., Kagemann, L., Fu, V., . . . Du, Y. (2014). A
731 laser-induced mouse model with long-term intraocular pressure elevation. *PLoS One,*
732 *9*(9), e107446. doi:10.1371/journal.pone.0107446
733 Yun, H., Wang, Y., Zhou, Y., Wang, K., Sun, M., Stolz, D. B., . . . Du, Y. (2018). Human
734 stem cells home to and repair laser-damaged trabecular meshwork in a mouse model.
735 *Commun Biol, 1*, 216. doi:10.1038/s42003-018-0227-z
736 Yun, H., Zhou, Y., Wills, A., & Du, Y. (2016). Stem Cells in the Trabecular Meshwork for
737 Regulating Intraocular Pressure. *J Ocul Pharmacol Ther, 32*(5), 253-260.
738 doi:10.1089/jop.2016.0005
739 Zadoo, S., Nguyen, A., Zode, G., & Hulleman, J. D. (2016). A Novel Luciferase Assay For
740 Sensitively Monitoring Myocilin Variants in Cell Culture. *Invest Ophthalmol Vis Sci,*
741 *57*(4), 1939-1950. doi:10.1167/iovs.15-18789
742 Zhou, Y., Grinchuk, O., & Tomarev, S. I. (2008). Transgenic mice expressing the Tyr437His
743 mutant of human myocilin protein develop glaucoma. *Invest Ophthalmol Vis Sci,*
744 *49*(5), 1932-1939. doi:10.1167/iovs.07-1339
745 Zhu, W., Gramlich, O. W., Laboissonniere, L., Jain, A., Sheffield, V. C., Trimarchi, J.
746 M., . . . Kuehn, M. H. (2016). Transplantation of iPSC-derived TM cells rescues
747 glaucoma phenotypes in vivo. *Proc Natl Acad Sci U S A, 113*(25), E3492-3500.
748 doi:10.1073/pnas.1604153113
749 Zode, G. S., Bugge, K. E., Mohan, K., Grozdanic, S. D., Peters, J. C., Koehn, D. R., . . .
750 Sheffield, V. C. (2012). Topical ocular sodium 4-phenylbutyrate rescues glaucoma in
751 a myocilin mouse model of primary open-angle glaucoma. *Invest Ophthalmol Vis Sci,*
752 *53*(3), 1557-1565. doi:10.1167/iovs.11-8837
753 Zode, G. S., Kuehn, M. H., Nishimura, D. Y., Searby, C. C., Mohan, K., Grozdanic, S.
754 D., . . . Sheffield, V. C. (2011). Reduction of ER stress via a chemical chaperone
755 prevents disease phenotypes in a mouse model of primary open angle glaucoma. *J*
756 *Clin Invest, 121*(9), 3542-3553. doi:10.1172/JCI58183
757

Stem Cell Transplantation Rescued A Primary Open-Angle Glaucoma Mouse Model

Siqi Xiong[1,2], Ajay Kumar[1], Shenghe Tian[1], Eman E. Taher[1,3,] Enzhi Yang[1], Paul R. Kinchington[1], Xiaobo Xia[2*], Yiqin Du[1,4,5*]

1. Department of Ophthalmology, University of Pittsburgh, Pittsburgh, PA 15213
2. Department of Ophthalmology, Xiangya Hospital, Central South University, Changsha, Hunan, China 410008
3. Research Institute of Ophthalmology, Giza, Egypt 12557
4. Department of Developmental Biology, University of Pittsburgh, Pittsburgh, PA 15213
5. McGowan Institute for Regenerative Medicine, University of Pittsburgh, Pittsburgh, PA 15213

*Corresponding authors:

Yiqin Du, duy@upmc.edu; 910 Eye and Ear Institute, 203 Lothrop St, Pittsburgh, PA 15213. Tel: 412-802-8437

Xiaobo Xia, xbxia21@163.com, 87 Xiangya Road, Changsha, Hunan, China 410008. Tel: 011-86-731-84327209

Supplemental Figures

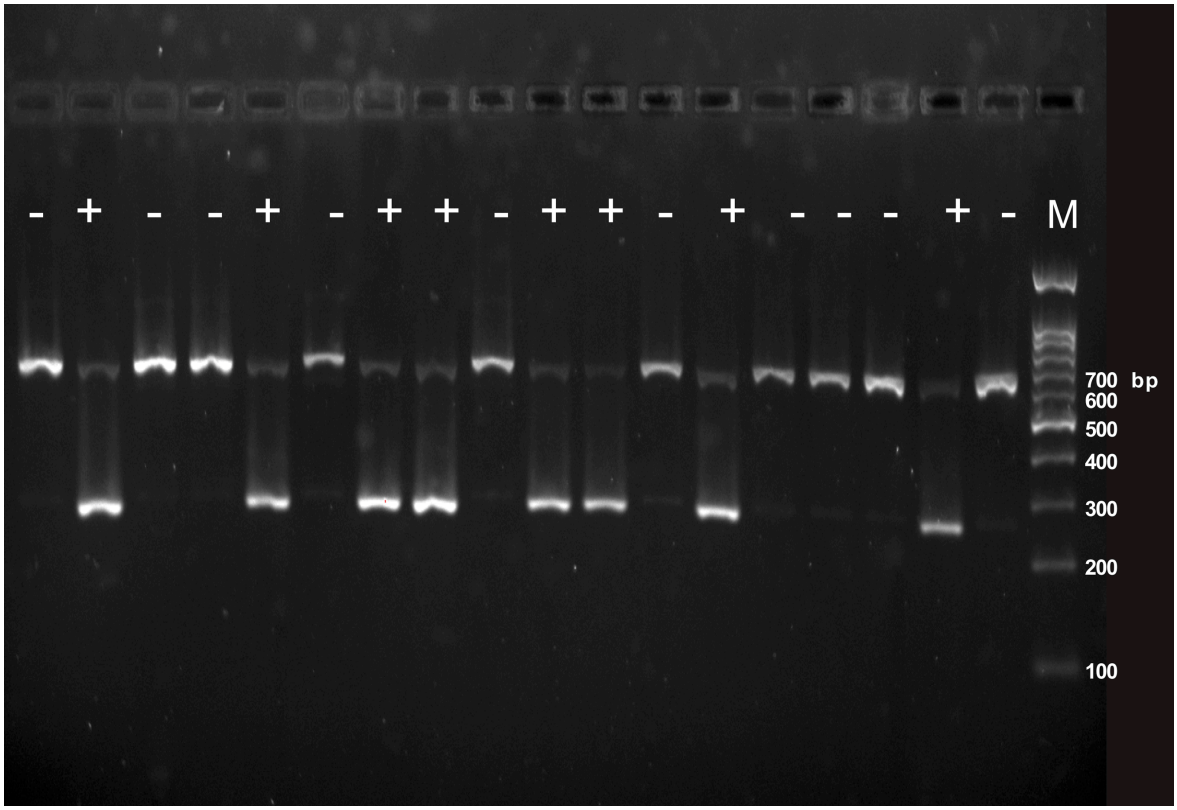

Figure S1. Genotyping of transgenic mice by polymerase chain reaction (PCR). Tg-Myoc Y437H mice (+) displayed with PCR products of 249 bp (MyocY437H) and weak band at 610 bp (mouse DNA). The mice with only 610 bp band were transgenic negative mice (-). M: DNA markers.

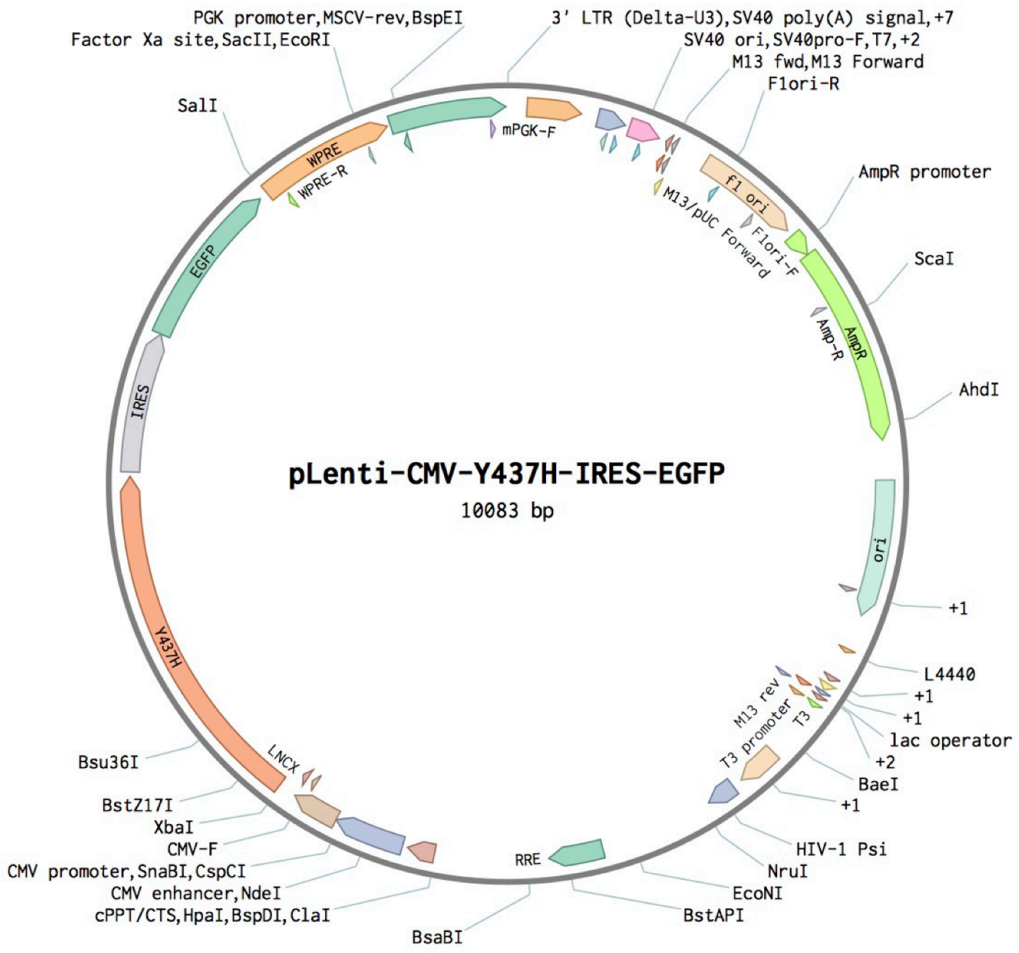

Figure S2. Structure of lentiviral packaging plasmid: pLenti$^{\text{CMV-Y437H-IRES-GFP}}$

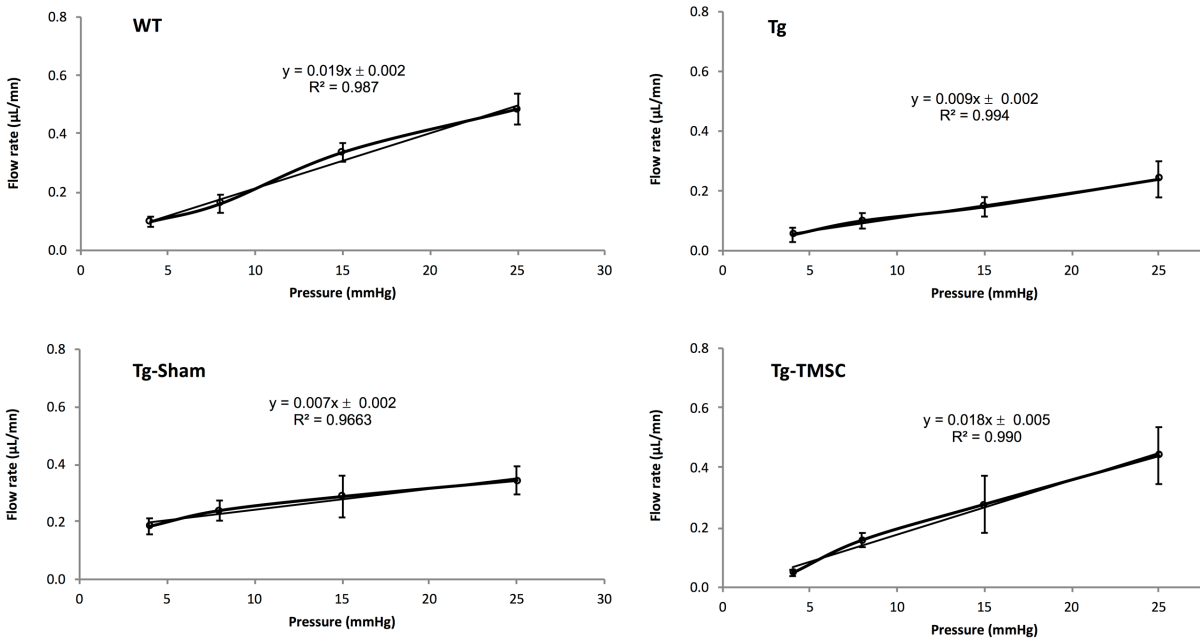

Figure S3. Representative perfusion outflow data from each mouse group. X-axis: perfusion pressure, Y-axis: flow rate, y is the slope indicating outflow facility (µL/min/mmHg).

Supplementary Tables

	Fibro-3	Fibro-2	Fibro-1	TMSC-3	TMSC-2	TMSC-1
HAPLN1	71.06156	246.6241	6.322361	1605.664	0.921353	7.638185
VTN	39.13535	26.4968	52.68634	36.58226	207.3045	654.0196
FST	5435.695	2775.031	5324.482	47082.35	9800.434	8603.46
COL4A5	1822.884	852.9932	1141.186	7856.286	8172.403	3951.806
COL4A6	189.4975	66.24201	80.08324	4491.708	5919.694	1349.094
LGALS3BP	705.4662	709.299	813.4771	3234.069	7502.579	6285.271
CHI3L1	48.40425	351.5922	22.12826	2131.658	482.7891	1541.959
LASP1	10996	10766.87	16347.52	10484.28	6723.114	8899.44
MYLK	2636.487	2302.165	1633.277	1357.498	397.1032	4418.69
TPM1	6461.453	11601.52	10073.63	4143.682	3928.65	13622.7
HSPG2	11474.9	9403.308	17417.05	6801.333	8018.537	17596.47
PDGFD	2599.411	868.2799	2079.003	125.5661	3435.726	5045.021
SLC12A2	7948.596	12497.32	4474.124	16198.03	6235.718	4524.67
SLC3A2	6396.571	4710.316	5036.814	6493.845	10527.38	8297.933
CYB5B	3445.971	3614.775	3453.063	7048.511	5787.941	3905.022
IL12B	4.119511	1.019108	33.71926	24.71774	6.449472	27.68842

Supplementary Table-1. Table showing related fold expression increase in (>1.5-fold change) genes related to TM ECM maintenance, TM integrity and motility, antioxidant defense, and immunosuppression in three individual TMSCs as compared to fibroblasts.

Annotated Pathway (KEGG)	Associated Genes
Focal adhesion	VTN, COL4A5, MYLK, PDGFD, and COL4A6
PI3K-Akt signaling pathway	VTN, COL4A5, PDGFD, and COL4A6
ECM-receptor interaction	VTN, COL4A5, HSPG2, and COL4A6
Proteoglycans in cancer	VTN, IL12B, and HSPG2
Protein digestion and absorption	COL4A5, SLC3A2, and COL4A6
Relaxin signaling pathway	COL4A5 and COL4A6
collagen type IV trimer	COL4A5 and COL4A6

Supplementary Table-2. Table showing list of top 7 annotated KEGG pathways, present in TMSC genes involved in ECM modulation. All manually curated metabolic and signaling pathways were imported from KEGG (June 2018), except collagen type IV trimer which was imported from gene complexes annotated by the Gene Ontology Consortium, as of September 2018.

	Fibro-3	Fibro-2	Fibro-1	TMSC-3	TMSC-2	TMSC-1
SELPLG	84.44997	60.12736	73.76088	43.50322	48.83172	51.55775
SLC16A6	36.04572	7.133755	3.16118	4.943548	0.921353	14.3216
ZFP36	189.4975	177.3248	283.4525	87.99515	119.7759	130.8039
MBP	2407.854	1104.713	1195.98	312.4322	403.5527	666.4316
IGF2	60.76279	39.7452	2.107454	5.932258	0	28.64319
CDH10	119.4658	74.39487	9.483541	5.932258	0.921353	0.954773
MMP10	18.5378	57.07004	4.214907	19.77419	0.921353	1.909546
EHD3	7359.506	3822.673	2708.078	1815.271	1850.999	1407.336
HLA-DPA1	53.55364	125.3503	25.28944	87.99515	14.74165	1.909546
BGN	472.7139	993.6301	201.2618	120.6226	355.6423	113.618

Supplementary Table-3. Table showing related fold expression increase in (>1.5-fold change) genes related to POAG in three individual fibroblasts as compared to TMSCs.

Fig1A Intraocular pressure(mmHg)

WT					
Baseline	Day 7	Day 14	Day 30	Day 60	Baseline
14	16	14	15	15	19
13	8	13	16	15	20
10	13	12	13	11	20
14	12	14	15	11	16
10	8	15	7	16	19
12	7	9	16	15	20
12	13	12	13	15	19
13	12	13	13	15	18
13	10	12	12	14	17
11	11	13	12	15	17
14	8	13	15	15	14
15	9	16	7	12	16
8	12	11	12	12	13
8	11	12	11	12	17
13	10	11	10	11	19
10	8	7	11	13	13
15	10	11	12	10	14
13	16	11	11	10	16
14	8	8	14	17	14
10	7	10	12	12	14
12	16	9	13	11	16
16	11	8	15	14	17
15	13	11	10	13	15
12	12	11	12	11	14
12	11	10	11	12	17
13	14	8	12	12	15

Fig1B Outflow facility(µL/min/mmHg)

WT	Tg	Tg-sham	Tg-TMSC
0.0141	0.0084	0.0111	0.019
0.0189	0.0086	0.0056	0.0258
0.014	0.0114	0.0152	0.0156
0.0185	0.01	0.0115	0.0122
0.0182	0.0112	0.0073	0.014
0.0182	0.0078	0.001	0.01

Fig1C Central corneal thickness(µm)

WT	Tg	Tg-sham	Tg-TMSC
96	91	109	102
91	109	108	103

99	95	100	92
103	91	95	89
102	93	100	101
91	110	105	113
91	91	110	97
92	93	112	105

Tg						Tg-sham
Day 7	Day 14	Day 30	Day 60	Baseline	Day 7	Day 14
18	16	12	10	17	17	16
17	19	12	8	16	17	17
20	14	15	15	21	18	15
18	13	15	16	19	18	16
15	16	15	13	14	19	11
16	18	13	15	15	13	17
17	17	9	11	13	22	17
18	19	20	15	14	19	18
13	18	18	13	16	19	15
16	15	21	18	15	18	17
16	18	11	16	18	19	16
14	21	10	19	18	21	17
15	14	18	15	16	20	17
16	15	21	19	14	14	18
17	18	13	18	19	14	13
15	15	12	15	18	17	13
14	19	19	14	13	13	17
16	17	14	18	14	19	17
15	17	19	16	19	20	19
17	13	17	11	19	13	21
13	16	15	19	16	14	14
12	15	16	21	15	21	15
19	17	17	12	13	11	16
20	14	13	13	14	11	17
15	17	15	13	17	16	18
14	14	16	16	15	17	13

		Tg-TMSC				
Day 30	Day 60	Baseline	Day 7	Day 14	Day 30	Day 60
15	16	19	21	15	14	11
16	16	20	19	17	14	12
16	17	20	19	14	13	11
16	15	16	17	15	14	13
16	14	19	18	14	14	13
15	15	20	17	14	14	15
13	16	19	17	16	12	12
13	16	18	17	18	18	13
16	15	17	17	16	16	17
16	15	17	19	15	15	14
16	15	18	19	18	12	11
15	15	18	17	19	14	11
15	16	14	16	12	16	12
15	15	10	16	12	11	12
16	13	13	12	9	10	10
15	13	12	17	13	9	10
14	17	10	13	17	14	15
14	16	11	13	14	13	14
19	16	12	16	13	11	11
18	16	13	15	18	14	14
20	15	12	17	19	12	12
21	15	14	19	16	10	12
15	14	12	11	20	17	16
15	14	14	10	13	12	15
19	17	12	13	10	14	12
17	16	13	14	11	13	11

FIg2B

The amplitute of pattern electroretinogram (μV)

WT	Tg	Tg-sham	Tg-TMSC
10.8	4.43	7.463	8.533
4.9	3.769	4.327	9.957
10.63	5.322	7.2	11.2
8.86	6.072	8.29	9.418
12.77	5.673	5.747	8.417
15.03	7.957	5.089	6.867
10.92	8.652	6.978	9.088
9.938	5.943	4.687	9.144
13.22	10.21	7.68	7.933
11.33	7.54	3.035	11.47

Fig3B TM cellularity(Cells/section)

WT	Tg	Tg-sham	Tg-TMSC
45	17	19	32
47	19	25	22
45	20	20	34
30	21	15	31
37	20	10	20
32	25	19	31
37	19	20	32
39	22	18	39
35	29	15	30
21	21	18	22
20	15	12	28
36	16	20	31
		11	30
			22

Fig4C

WT	Tg	Tg-sham	Tg-TMSC
0.16	0.89	1.47	0.81
0.03	0.56	0.82	0.08
0.07	1.06	1.49	0.34
0.33	0.55	0.48	0.29
0.19	0.63	0.61	0.21

Fig4E

WT	Tg	Tg-sham	Tg-TMSC
1.08	0.32	0.14	0.56
0.92	0.77	0.5	0.98
0.99	0.08	0.25	0.72
1.25	0.21	0.02	0.51
0.76	0.08	0.25	0.65

FIg4G

Fibronectin				Collagen IV	
WT	Tg	Tg-sham	Tg-TMSC	WT	Tg
0.34	1.11	1.44	0.69	0.5	0.45
0.76	0.72	0.87	0.45	0.91	0.57
0.52	1.23	1.65	0.69	0.93	0.66
0.57	0.82	0.83	0.41	0.37	0.57
0.59	0.65	0.6	0.58	0.89	0.68
0.81	0.94	0.8	0.67	0.74	0.68

Elastin					
Tg-sham	Tg-TMSC	WT	Tg	Tg-sham	Tg-TMSC
0.78	0.7	0.27	0.56	0.69	0.26
0.9	0.32	0.23	0.63	0.53	0.16
0.7	0.67	0.12	0.57	0.57	0.19
0.93	0.57	0.19	0.59	0.64	0.17
0.7	0.69				
0.59	0.89				

FIg5B

Chop				Grp78	
WT	Tg	Tg-sham	Tg-TMSC	WT	Tg
0.24	0.93	0.72	0.51	1.08	1.48
0.47	0.88	0.74	0.35	1.12	1.53
0.24	0.8	1.14	0.95	1.13	1.78
0.63	1.21	0.77	1.06	1.19	1.6
0.6	0.65	0.53	0.5	0.57	0.89
0.37	0.68	0.41	0.68	0.65	0.9

Tg-sham	Tg-TMSC
1.68	1.5
1.64	1.29
1.85	1.63
1.77	1.34
0.64	0.57
0.64	0.66

Fig6B

Y437H TM	Y437H TM+TMSC	Y437H TM+TMSC Contact
3.16	9.63	9.18
8.82	4.37	6.79
4.67	4.19	3.56
9.4		
6.59		

Fig6D

Grp78

TM	Y437H TM	GFP TM
0.69	1.21	0.77
0.71	1.42	0.69
0.57	1.33	0.63

Chop

TM	Y437H TM	GFP TM
0.07	0.24	0.05
0.1	0.21	0.03
0.03	0.19	0.07

Myocilin

TM	Y437H TM	GFP TM
0.1	0.91	0.04
0.12	0.89	0.11
0.09	0.97	0.02

TMSC		
TM	Y437H TM	GFP TM
0.82	1.33	0.66
0.72	1.27	0.71
0.76	1.21	0.59

TMSC		
TM	Y437H TM	GFP TM
0.02	0.13	0.05
0.04	0.37	0.13
0.07	0.21	0.03

TMSC		
TM	Y437H TM	GFP TM
0.16	1.01	0.09
0.09	0.89	0.16
0.13	0.93	0.09

Fig7A

CHI3L1

TMSC	TM+TMSC	Y437H TM+TMSC
0.17	0.47	0.62
0.21	0.65	0.72
0.11	0.56	0.53

Fig7B

Myocilin

TMSC	TM+TMSC	Y437H TM+TMSC
0.12	0.46	0.53
0.16	0.51	0.43
0.14	0.42	0.57

Fig7D

Phagocytosis

TMSC	TM+TMSC	Y437H TM+TMSC
22	80	86
33	57	76
30	83	64
16	70	77
33	75	81
41	90	76
23	87	70
12	60	75
55	75	78
20	45	50